AWARD NUMBER: W81XWH-17-1-0129

TITLE: Targeting the Cell Surfaceome of Aggressive Neuroendocrine Prostate Cancer

PRINCIPAL INVESTIGATOR: John K. Lee, M.D., Ph.D.

CONTRACTING ORGANIZATION: Fred Hutchinson Cancer Research Center
Seattle, WA 98109

REPORT DATE: JULY 2019

TYPE OF REPORT: Annual Technical Report

PREPARED FOR: U.S. Army Medical Research and Materiel Command
Fort Detrick, Maryland 21702-5012

REPORT DOCUMENTATION PAGE

Form Approved
OMB No. 0704-0188

1. REPORT DATE	2. REPORT TYPE	3. DATES COVERED
JULY 2019	Annual Technical Report	1JUL2018 – 30JUN2019

4. TITLE AND SUBTITLE
Targeting the Cell Surfaceome of Aggressive Neuroendocrine Prostate Cancer

5a. CONTRACT NUMBER
W81XWH-17-1-0129

5b. GRANT NUMBER

5c. PROGRAM ELEMENT NUMBER

6. AUTHOR(S)
John K. Lee, M.D., Ph.D.

E-Mail: jklee5@fredhutch.org

5d. PROJECT NUMBER

5e. TASK NUMBER

5f. WORK UNIT NUMBER

7. PERFORMING ORGANIZATION NAME(S) AND ADDRESS(ES)
Fred Hutchinson Cancer Research Center

1100 Fairview Ave N, J6-300
Seattle, WA 98109-4433

8. PERFORMING ORGANIZATION REPORT NUMBER

9. SPONSORING / MONITORING AGENCY NAME(S) AND ADDRESS(ES)

U.S. Army Medical Research and Materiel Command
Fort Detrick, MD 21702-5012

10. SPONSOR/MONITOR'S ACRONYM(S)

11. SPONSOR/MONITOR'S REPORT NUMBER(S)

12. DISTRIBUTION / AVAILABILITY STATEMENT

Approved for Public Release; Distribution Unlimited

13. SUPPLEMENTARY NOTES

14. ABSTRACT
In this reporting period, we have generated and validated lentiviral constructs in anticipation of studies evaluating the cooperation of MYCN overexpression with TP53 and RB1 loss in the initiation of neuroendocrine prostate cancer (NEPC). We have continued validating candidate NEPC cell surface antigens arising from integrated transcriptome and cell surface proteome analysis of prostate cancer cell lines. CEACAM5 (carcinoembryonic antigen related cell adhesion molecule 5) was previously characterized as a cell surface marker enriched in NEPC. We also identified L1CAM (L1 cell adhesion molecule) and validation of L1CAM expression in patient-derived xenograft and archived clinical NEPC biospecimens is ongoing. In the next phase of our studies, we are evaluating a clinical-grade CEACAM5 antibody-drug conjugate in preclinical CEACAM5-postive NEPC models. In addition, we will start the process of humanizing an available chimeric mouse/human antibody targeting L1CAM that has shown preclinical therapeutic activity in various L1CAM-expressing cancer models.

15. SUBJECT TERMS
Neuroendocrine prostate cancer, cell surface antigens, antibody therapy, immunotherapy

16. SECURITY CLASSIFICATION OF:			17. LIMITATION OF ABSTRACT	18. NUMBER OF PAGES	19a. NAME OF RESPONSIBLE PERSON
a. REPORT	b. ABSTRACT	c. THIS PAGE			USAMRMC
Unclassified	Unclassified	Unclassified	Unclassified	43	19b. TELEPHONE NUMBER *(include area code)*

Table of Contents

INTRODUCTION

Background: Neuroendocrine prostate cancer (NEPC) is a common, deadly endpoint for men with late-stage metastatic prostate cancer. Up to 20% of men with lethal metastatic prostate cancers demonstrate evidence of NEPC [1, 2]. NEPC can be distinguished from conventional prostate cancer or prostate adenocarcinoma (PrAd) by histologic features, neuroendocrine marker expression, loss of either androgen receptor (AR) or downstream AR signaling, Polycomb repressive complex expression, and global methylation patterns [3-5]. Genomic studies of NEPC have also identified frequent amplification of *MYCN* and loss of both *TP53* and *RB1* [5, 6]. NEPC represents a cancer differentiation state distinct from PrAd and we hypothesize that the cell surface phenotype of these prostate cancer subtypes should reflect these differences. Furthermore, these differences in cell surface antigen expression may provide an opportunity for prostate cancer subtype-specific therapeutic targeting. The purpose of the research is to establish new NEPC models, to characterize the differential cell surface antigen profile of NEPC relative to PrAd, and to develop antibody reagents targeting novel antigens in NEPC. We believe that these studies may facilitate the development of targeted treatments for men with NEPC, for which there are no currently available FDA-approved therapeutics.

KEYWORDS

Neuroendocrine prostate cancer, cell surface antigens, antibody therapy, immunotherapy

ACCOMPLISHMENTS

To summarize the research accomplishments to date, the tasks described in the proposed Statement of Work are itemized here with a brief update for each task.

SA 1: Establish a diverse panel of NEPC cell lines from human prostate epithelial transformation (months 1-12)

Task 1: Use the human prostate organoid transformation assay with the oncogenes MYCN and activated AKT1 to generate new NEPC cell lines (months 1-12) Completed during the previous reporting period.

Task 2: Evaluate the effect of p53 loss and Rb loss in combination with the oncogenes MYCN and activated AKT1 in initiation of NEPC (months 1-24) In progress. Colleagues and I have evaluated the combination of c-Myc, activated AKT1, mutant p53 R175H, and a short-hairpin targeting Rb1 (shRb1) in the human prostate epithelial assay which generates penetrant small cell NEPC phenotype (Appendix 1, Fig. 1A-D). Initiation of small cell NEPC within this system is dependent on disruption of p53 and Rb as the absence of mutant p53 R175H and shRb1 initiate tumors with prostate adenocarcinoma histology (Appendix 1, Fig. 1D). We have cloned a 3rd-generation lentiviral vector that co-expresses *MYCN* and *BCL2* and verified protein expression after transfection of HEK 293T cells (Fig. 1A). Batches of VSV-G pseudotyped FU-MYCN-P2A-BCL2-CRW, FU-myrAKT1-CGW, and FU-TP53DN-shRB1-CYW lentiviruses have been produced and their infectious titers determined on HEK 293T cells (Fig. 1B). We are awaiting local IRB review and approval prior to initiating these experiments which require the use of de-identified, viable prostate tissue biospecimens obtained through the University of Washington (UW) Genitourinary Cancer Specimen Repository from patients undergoing prostatectomy at the UW Medical Center.

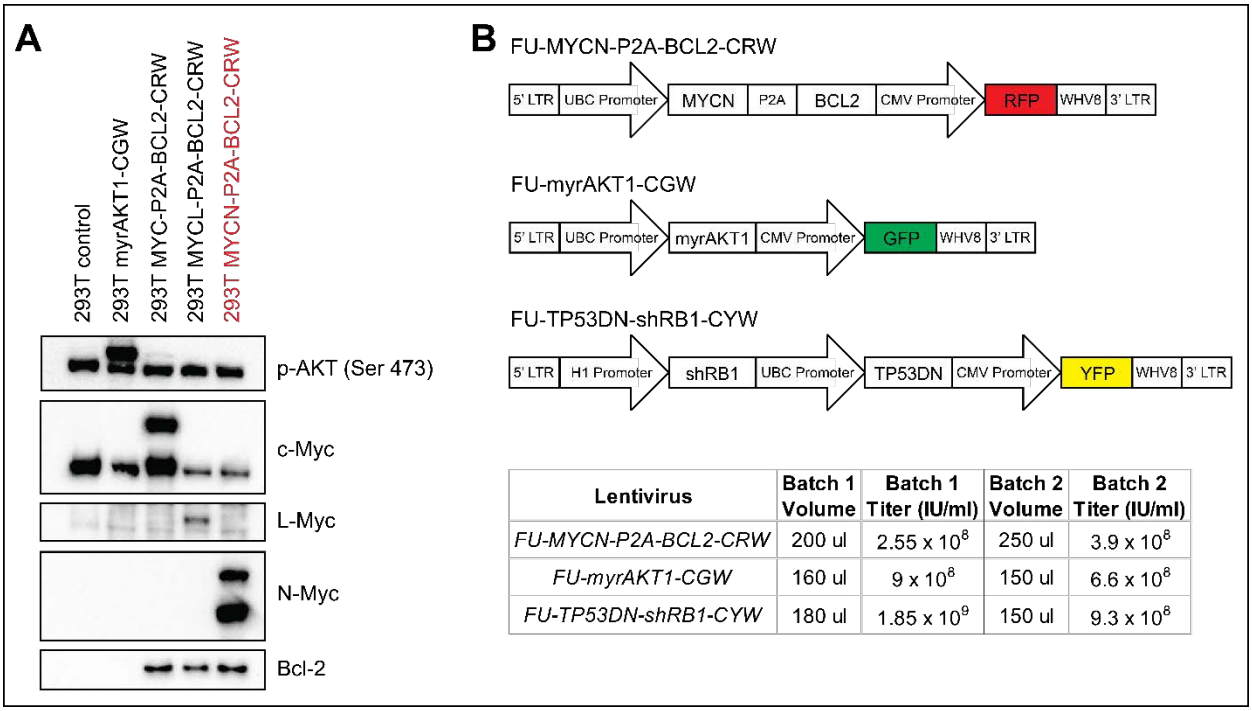

Lentivirus	Batch 1 Volume	Batch 1 Titer (IU/ml)	Batch 2 Volume	Batch 2 Titer (IU/ml)
FU-MYCN-P2A-BCL2-CRW	200 ul	2.55×10^8	250 ul	3.9×10^8
FU-myrAKT1-CGW	160 ul	9×10^8	150 ul	6.6×10^8
FU-TP53DN-shRB1-CYW	180 ul	1.85×10^9	150 ul	9.3×10^8

Fig. 1. Validation and production of polycistronic lentiviruses for proposed human prostate epithelial transformation studies. (**A**) Western blot analysis of lysates from HEK 293T cells transfected with various constructs including FU-MYCN-P2A-BCL2-CW using antibodies to validate overexpression of the specified proteins. (**B**) *Top*, basic schematics of the lentiviral vectors. LTR=long terminal repeat; UBC=Ubiquitin C; CMV=cytomegalovirus; WHV8=Woodchuck hepatitis virus 8 posttranscriptional regulatory element. *Bottom*, volumes and infectious titers on HEK 293T cells (infectious units per milliliter) of the specified lentiviruses from two independent production batches.

SA 2: Validate candidate cell surface markers on NEPC using proteomic approaches

Task 1: High-throughput cell surface proteomic analysis of prostate cancer cell lines (months 1-14) Completed during the previous reporting period.

Task 2: Validation of candidate cell surface proteins using low-throughput proteomic techniques (months 6-18) In progress. Multi-level validation of candidate NEPC cell surface marker expression by immunoblotting and immunohistochemistry of NEPC cell lines, xenografts, and archived tumors continues. Part of these results were published last year in *Lee JK, et al. PNAS, 2018* with a specific focus on carcinoembryonic antigen related cell adhesion molecule 5 (CEACAM5) which was in validation studies to be expressed in approximately 60% of NEPC tumors analyzed. Cooperative studies with Dr. Pete Nelson's laboratory at Fred Hutch also identified L1 cell adhesion molecule (L1CAM) as another promising cell surface antigen whose expression is enriched in NEPC (Fig. 2A-B). Further characterization of L1CAM expression in patient-derived xenograft models and archived clinical specimens is ongoing and is consistent with our initial analysis.

Task 3: Prioritization of candidate NEPC cell surface proteins for therapeutic development (months 6-18) In progress. We have attempted to prioritize candidate antigens based partly on the criteria of limited systemic expression in normal tissues. However, this is highly prohibitive as we have found that surface antigens enriched in NEPC are expressed to some degree in normal tissues as well. Our leading target cell surface antigens in NEPC are CEACAM5 and L1CAM at this juncture. We and others have shown CEACAM5 expression in the epithelial lining of the gastrointestinal tract [7]. L1CAM expression is upregulated in multiple metastatic cancers [8-11] and associated with the

process of epithelial-to-mesenchymal transition [12] but is also widely expressed in normal neuronal tissues. While seemingly problematic, a therapeutic antibody that recognizes the glycosylation-dependent CE7 epitope of L1CAM has demonstrated tumor selectivity [13]. Another consideration is that antibodies and antibody-drug conjugates (ADC) targeting broadly expressed antigens have been found to be tolerable in humans with poor correlation between dose-limiting toxicities and tissue sites of antigen expression [14].

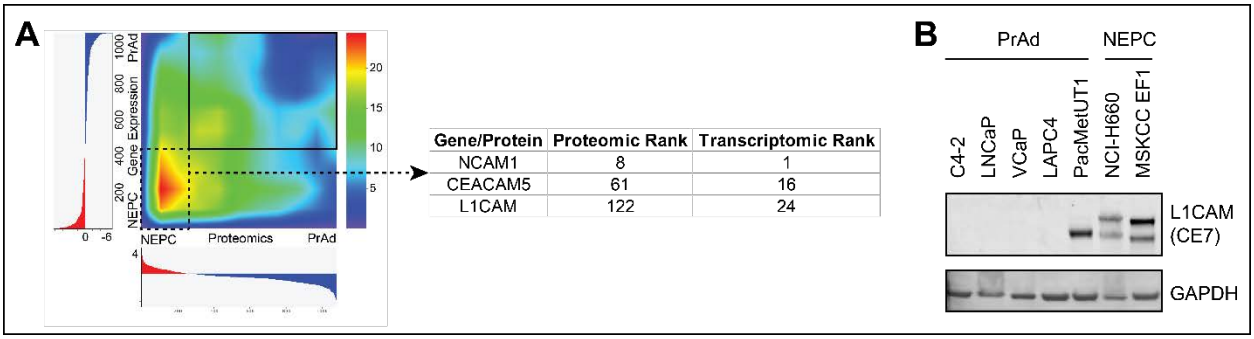

Gene/Protein	Proteomic Rank	Transcriptomic Rank
NCAM1	8	1
CEACAM5	61	16
L1CAM	122	24

Fig. 2. L1CAM as a potential cell surface antigen enriched in NEPC. (**A**) Data from *Lee JK, et al. PNAS, 2018* showing the proteomic rank and transcriptomic rank of NCAM1, CEACAM5, and L1CAM enrichment in NEPC cell lines relative to prostate adenocarcinoma (PrAd) cell lines. (**B**) Western blot analysis of L1CAM expression detected by the glycosylation-dependent CE7 antibody in PrAd and NEPC cell lines.

SA 3: Develop novel antibody reagents targeting cell surface antigens in NEPC (months 18-48)

Task 1: Human scFv phage display library screening to identify antibody reagents (months 18-32) In progress. CEACAM5 and L1CAM are glycosyl phosphatidyl inositol (GPI)-anchored membrane proteins for which therapeutic antibodies have previously been developed. The use of these or variants of these antibodies would represent a significantly accelerated starting point to evaluate the therapeutic targeting of these cell surface antigens in NEPC without requiring new antibody reagent discovery. In the case of CEACAM5, we have engaged in a sponsored research agreement with Immunomedics, Inc. to use their investigational anti-CEACAM5 antibody labetuzumab govitecan to evaluate therapeutic efficacy in preclinical models of NEPC. Labetuzumab is a fully human monoclonal antibody with nanomolar affinity for CEACAM5 and labetuzumab govitecan has been investigated in a phase I/II study in patients with refractory/relapsed metastatic colorectal cancer [15]. Labetuzumab govitecan treatment was safe, tolerable, and associated with a median survival that exceeded matched, historic controls by approximately 4 months. With regard to L1CAM, the murine CE7 antibody that binds the glycosylation-dependent CE7 epitope of L1CAM in neuroblastoma was first reported over three decades ago [16]. Since then, a mouse/human chimeric CE7 antibody has been developed [17] and the single chain variable fragment (scFv) of CE7 has been incorporated into chimeric antigen receptors (CARs) that are under clinical investigation for the treatment of relapsed/refractory neuroblastoma at Seattle Children's Hospital [18]. We are currently reviewing a commercial antibody humanization strategy from Creative Biolabs, Inc. to perform 1) full humanization of the chCE7 antibody by structural modeling and optimization of complementarity-determining region (CDR) grafting into a human antibody acceptor framework and 2) expression and validation of humanized antibodies for binding to target NEPC cell lines that have been genetically engineered to control for expression of L1CAM.

Task 2: Validation of the specificity and performance of human monoclonal antibodies derived from phage display screening (months 18-34) Not yet started.
Task 3: Therapeutic evaluation of monoclonal antibodies against candidate cell surface targets (months 30-40) Not yet started.
Task 4: Mouse studies with therapeutic monoclonal antibodies in NEPC (months 40-48) Not yet started.

Key Research Accomplishments:

- Generation and validation of lentiviral reagents for proposed human prostate epithelial transformation assays to generate novel models of NEPC.

- Putative NEPC cell surface antigens have been identified through a multi-level strategy involving integration of transcriptome and cell surface proteome data and low-throughput validation. Examples of these include CEACAM5 and L1CAM which have not been previously considered as significant prostate cancer antigens.

Opportunities for Training and Professional Development:

This reporting period includes a large portion of my first year as an independent investigator in the Prostate Cancer Program in the Human Biology Division at Fred Hutch. My laboratory now includes two post-doctoral fellows, a graduate student, and two technicians that I oversee and mentor. Establishing a laboratory has provided many ongoing learning experiences related to leadership, organization, personnel management, and resource utilization. I have developed a local mentoring network at Fred Hutch through the establishment of a junior faculty mentoring committee consisting of Drs. Pete Nelson, Valeri Vasioukhin, and Bob Eisenman. I have also maintained broader networks through my involvement with the Prostate Cancer Foundation and the Pacific Northwest Prostate Cancer SPORE. I stepped down as a co-leader of the Prostate Cancer Foundation Young Investigator Tumorigenesis Working Group but recently took on the role of co-leader of the Microenvironment and Immunology Working Group. The scientific progression of this project has importantly allowed me to develop productive interactions with industry (Immunomedics, Inc.) that will fast-track the evaluation of antibody therapies in NEPC.

Dissemination of Results:

Recent results pertaining to these studies have been disseminated to the regional prostate cancer research community through a talk at the Pacific Northwest Prostate Cancer SPORE seminar series on April 4, 2019 held at Fred Hutch but also broadcast to the Oregon Health Sciences University and the Vancouver Prostate Centre of the University of British Columbia.

Plan for the Next Reporting Period:

In the next reporting period, we will have received IRB approval to perform human prostate organoid transformation studies evaluating the effect of *TP53* and *RB1* loss in combination with the oncogenes *MYCN* and activated *AKT1* in initiation of NEPC from Specific Aim 1, Task 2. We will complete low-throughout proteomic validation studies and focus on the development/evaluation of targeted antibody reagents revolving around CEACAM5 and L1CAM. We will continue

studies related to defining the activity of labetuzumab govitecan in preclinical NEPC models and proceed with humanization of the chCE7 antibody targeting L1CAM.

IMPACT

The impact of our discovery and validation of CEACAM5 expression in NEPC has prompted multiple additional areas of investigation. We have previously engineered a CEACAM5 chimeric antigen receptor T cell immunotherapy that demonstrates antigen-specific NEPC killing [7]. These studies led to a Prostate Cancer Foundation Team Science Challenge Award (PI's: Drs. Owen Witte, John Lee, Stephen Forman, and Saul Priceman) to investigate the safety and efficacy of CEACAM5 CAR T cell immunotherapy for NEPC in clinically relevant immune-competent mouse models. In addition, we have established a sponsored research agreement with Immunomedics, Inc. to evaluate the anti-CEACAM5 ADC named labetuzumab govitecan in cell line and patient-derived xenograft models of NEPC. If the results from these studies are compelling, this would represent a discrete path to the rapid translation of our findings into the clinic as we would propose an investigator-initiated clinical trial of labetuzumab govitecan in CEACAM5-positive NEPC.

The finding of L1CAM expression in NEPC has also led to significant interactions with prominent pediatric oncologists at Seattle Children's Hospital including Drs. Michael Jensen, Julie Park, and Navin Pinto as they have focused on clinical targeting of L1CAM in neuroblastoma using CAR T cell immunotherapy for over a decade. As they have generated and vetted the preclinical safety, specificity, and potency of these agents, we have proposed to pursue preclinical and clinical studies evaluating L1CAM CAR T cell therapy in NEPC. This idea has formed the basis for a Prostate Cancer Foundation Team Science Challenge Award application (PI's: Drs. John Lee, Pete Nelson, Michael Jensen, Julie Park, and Vicki Wu) that we recently submitted.

CHANGES/PROBLEMS

The project was impacted by my relocation from UCLA to Fred Hutchinson Cancer Research Center and the non-trivial task of establishing a new laboratory. However, I believe that we will still be able to achieve the proposed milestones in a timely manner.

One change to the project, as outlined above, relates to pre-existing therapeutic antibodies for cell surface antigens that we validate in NEPC. While we initially proposed to generate new antibody reagents against these antigens, the use of existing or modifications of existing antibody reagents may also accelerate preclinical investigation and shorten the potential road to clinical translation.

PRODUCTS

Publication: Park JW, Lee JK, Sheu KM, Wang L, Balanis NG, Nguyen K, Smith BA, Cheng C, Tsai BL, Cheng D, Huang J, Kurdistani SK, Graeber TF, Witte ON. Reprogramming normal human epithelial tissues to a common, lethal neuroendocrine cancer lineage. Science. 2018 Oct 5;362(6410):91-95.

PARTICIPANTS & OTHER COLLABORATING ORGANIZATIONS

Name:	*John K. Lee*
Project Role:	*PI*
Researcher Identifier (e.g. ORCID ID):	https://orcid.org/0000-0002-6570-2180
Nearest person month worked:	*3*
Contribution to Project:	*Dr. Lee has performed data analysis and overseen the conduct of the study.*
Funding Support:	

Name:	*Tiffany Pariva*
Project Role:	*Research Technician*
Researcher Identifier (e.g. ORCID ID):	
Nearest person month worked:	*5*
Contribution to Project:	*Ms. Pariva has performed low-throughput proteomic analyses to validate the expression of candidate prostate cancer subtype-specific antigens in cell lines, xenografts, and archived clinical tissues.*
Funding Support:	

SPECIAL REPORTING REQUIREMENTS

Nothing to Report.

REFERENCES

1. Tanaka, M., et al., *Progression of prostate cancer to neuroendocrine cell tumor.* Int J Urol, 2001. **8**(8): p. 431-6; discussion 437.
2. Bluemn, E.G., et al., *Androgen Receptor Pathway-Independent Prostate Cancer Is Sustained through FGF Signaling.* Cancer Cell, 2017. **32**(4): p. 474-489.e6.
3. Yao, J.L., et al., *Small cell carcinoma of the prostate: an immunohistochemical study.* Am J Surg Pathol, 2006. **30**(6): p. 705-12.
4. Clermont, P.L., et al., *Polycomb-mediated silencing in neuroendocrine prostate cancer.* Clin Epigenetics, 2015. **7**: p. 40.
5. Beltran, H., et al., *Divergent clonal evolution of castration-resistant neuroendocrine prostate cancer.* Nat Med, 2016. **22**(3): p. 298-305.
6. Beltran, H., et al., *Molecular characterization of neuroendocrine prostate cancer and identification of new drug targets.* Cancer Discov, 2011. **1**(6): p. 487-95.
7. Lee, J.K., et al., *Systemic surfaceome profiling identifies target antigens for immune-based therapy in subtypes of advanced prostate cancer.* Proc Natl Acad Sci U S A, 2018. **115**(19): p. E4473-e4482.
8. Euer, N.I., et al., *Identification of L1CAM, Jagged2 and Neuromedin U as ovarian cancer-associated antigens.* Oncol Rep, 2005. **13**(3): p. 375-87.
9. van der Putten, L.J., et al., *L1CAM expression in endometrial carcinomas: an ENITEC collaboration study.* Br J Cancer, 2016. **115**(6): p. 716-24.
10. Altevogt, P., K. Doberstein, and M. Fogel, *L1CAM in human cancer.* Int J Cancer, 2016. **138**(7): p. 1565-76.
11. Tischler, V., et al., *L1CAM protein expression is associated with poor prognosis in non-small cell lung cancer.* Mol Cancer, 2011. **10**: p. 127.
12. Kiefel, H., et al., *L1CAM: a major driver for tumor cell invasion and motility.* Cell Adh Migr, 2012. **6**(4): p. 374-84.
13. Arlt, M.J., et al., *Efficient inhibition of intra-peritoneal tumor growth and dissemination of human ovarian carcinoma cells in nude mice by anti-L1-cell adhesion molecule monoclonal antibody treatment.* Cancer Res, 2006. **66**(2): p. 936-43.
14. Hinrichs, M.J. and R. Dixit, *Antibody Drug Conjugates: Nonclinical Safety Considerations.* Aaps j, 2015. **17**(5): p. 1055-64.
15. Dotan, E., et al., *Phase I/II Trial of Labetuzumab Govitecan (Anti-CEACAM5/SN-38 Antibody-Drug Conjugate) in Patients With Refractory or Relapsing Metastatic Colorectal Cancer.* J Clin Oncol, 2017. **35**(29): p. 3338-3346.
16. Schonmann, S.M., et al., *Production and characterization of monoclonal antibodies against human neuroblastoma.* Int J Cancer, 1986. **37**(2): p. 255-62.
17. Amstutz, H., et al., *Production and characterization of a mouse/human chimeric antibody directed against human neuroblastoma.* Int J Cancer, 1993. **53**(1): p. 147-52.
18. Park, J.R., et al., *Adoptive transfer of chimeric antigen receptor re-directed cytolytic T lymphocyte clones in patients with neuroblastoma.* Mol Ther, 2007. **15**(4): p. 825-33.

APPENDICES

Appendix 1: Park JW, Lee JK, Sheu KM, Wang L, Balanis NG, Nguyen K, Smith BA, Cheng C, Tsai BL, Cheng D, Huang J, Kurdistani SK, Graeber TF, Witte ON. Reprogramming normal human epithelial tissues to a common, lethal neuroendocrine cancer lineage. Science. 2018 Oct 5;362(6410):91-95.

CANCER

Reprogramming normal human epithelial tissues to a common, lethal neuroendocrine cancer lineage

Jung Wook Park[1], John K. Lee[2], Katherine M. Sheu[3], Liang Wang[1], Nikolas G. Balanis[3], Kim Nguyen[4], Bryan A. Smith[1], Chen Cheng[5], Brandon L. Tsai[1], Donghui Cheng[1], Jiaoti Huang[6], Siavash K. Kurdistani[5,7,8,9], Thomas G. Graeber[3,7,8,9,10]*, Owen N. Witte[1,3,7,8,9]*

The use of potent therapies inhibiting critical oncogenic pathways active in epithelial cancers has led to multiple resistance mechanisms, including the development of highly aggressive, small cell neuroendocrine carcinoma (SCNC). SCNC patients have a dismal prognosis due in part to a limited understanding of the molecular mechanisms driving this malignancy and the lack of effective treatments. Here, we demonstrate that a common set of defined oncogenic drivers reproducibly reprograms normal human prostate and lung epithelial cells to small cell prostate cancer (SCPC) and small cell lung cancer (SCLC), respectively. We identify shared active transcription factor binding regions in the reprogrammed prostate and lung SCNCs by integrative analyses of epigenetic and transcriptional landscapes. These results suggest that neuroendocrine cancers arising from distinct epithelial tissues may share common vulnerabilities that could be exploited for the development of drugs targeting SCNCs.

Human cancers originating in different organs share commonalities in cancer phenotypes and molecular features (*1*). Small cell neuroendocrine carcinoma (SCNC) is recognized by its distinctive histological features and can arise from almost all epithelial organs, including the prostate and lung (*2*, *3*). These cancers show notable lineage plasticity and acquire therapeutic resistance by converting from an epithelial to a neuroendocrine cancer phenotype (*4*–*8*). Large-scale analyses of transcriptome data from a variety of cancer types have provided substantial evidence (*9*–*11*) to support a phenotypic convergence to SCNC during cancer progression. The underlying molecular mechanisms are not fully understood.

To explore whether distinct human epithelial cell types can be transformed into SCNC by shared oncogenic drivers, we used a human tissue transformation assay (*12*). Small cell prostate cancer (SCPC) is a type of neuroendocrine prostate cancer (NEPC), a class of malignancies that includes the extremely rare "large cell prostate carcinoma," whose exact definition is still emerging (*13*). Overexpression of c-Myc or N-Myc in combination with myristoylated AKT1 (myrAKT1) (a partial mimic of *PTEN* loss) drives normal human prostate epithelial cells to poorly differentiated prostate adenocarcinoma (PrAd) or SCPC, respectively (*12*, *14*). To identify additional oncogenic drivers of SCPC, we investigated the functional effects of dominant negative p53 (TP53DN) (P), myrAKT1 (A), *RB1*–short hairpin RNA (shRNA) (R), c-Myc (C), and BCL2 (B) on the genesis of SCPC on the basis of their recurrent genetic alterations in prostate cancers, including SCPC (*5*, *7*, *15*, *16*). These five genetic factors are hereafter referred to as PARCB. Primary basal epithelial cells were isolated from the prostates of eight human donors and were lentivirally transduced with the PARCB factors, briefly cultured in an organoid system (Fig. 1A), and transplanted into immunodeficient NOD/SCID-IL2R-γc-KO mice (*17*), where they formed tumors that displayed green, red, and yellow fluorescent protein (GFP, RFP, and YFP) expression from the three lentiviruses (Fig. 1B). PARCB gene expression and the human cellular origin of the tumors were confirmed by immunostaining (fig. S1). All PARCB tumors derived from basal cells demonstrated histological features of human SCPC, including a high nuclear-to-cytoplasmic ratio, frequent mitotic and apoptotic figures, and uniform expression of neuroendocrine differentiation (NED) markers (Fig. 1, C and D).

We next defined the genetic factors required to initiate SCPC from the PARCB combination by leave-one-out analysis. No tumors developed in the absence of either c-Myc or myrAKT1. In the absence of BCL2, the PARC combination still produced tumors with histologic characteristics and NED marker expression consistent with SCPC (Fig. 1D and fig. S2A), albeit with reduced efficiency (fig. S3). In contrast to BCL2, *RB1*-shRNA and TP53DN together or individually were indispensable for SCPC development. Tumors arising from these conditions—PACB (without *RB1*-shRNA), ARCB (without TP53DN), and ACB (without TP53DN and *RB1*-shRNA)—displayed histological features of poorly differentiated PrAd. PACB and ARCB tumors displayed only focal expression of NED markers (Fig. 1D). Thus, loss of *RB1* and inactivation of p53 are required to convert an epithelial lineage into a neuroendocrine lineage in SCPC development during human prostate epithelial transformation.

To further investigate the molecular contributions of the PARCB genetic factors to SCPC, we established tumor cell lines from fluorescence-activated cell sorting (FACS)–purified cells of the ACB, PACB, ARCB, and PARCB tumors (Fig. 2A). Immunoblot analysis confirmed the expression of the respective genetic factors in the newly generated cell lines (fig. S2B). We then performed two downstream global analyses: mRNA sequencing (RNA-seq) and assay for transposase-accessible chromatin sequencing (ATAC-seq). Currently, gene expression datasets specific for SCPC are lacking. We used the largest available RNA-seq dataset of NEPC and PrAd patient samples (*8*) in our study. We simplified the nomenclature of NEPC as SCPC to prevent confusion when alternating between epithelial tissue types.

Our RNA-seq data revealed that the PARCB cell lines have transcriptomes that are distinct from those characterizing ACB, PACB, and ARCB lines (fig. S4A), supporting the histologic and molecular differences described above. The PARCB cell lines exhibited enriched expression of genes that are up-regulated in clinical SCPC specimens relative to PrAd samples (*8*, *18*), whereas the ACB, PACB, and ARCB lines did not (fig. S5A). The PARCB lines were also highly similar to human SCPC (fig. S5B) on the basis of a published SCPC gene expression signature (*7*).

Global transcriptome analysis revealed that the PARCB cell lines exhibited strong transcriptional similarity to SCPC patient samples, whereas the other engineered cell lines clustered with patient-derived PrAd cell lines (Fig. 2B). They did not express detectable levels of androgen receptor (AR) and exhibited the lowest level of AR signaling activity when compared with clinical samples (fig. S6). The PARCB cell lines also exhibited NED markers in vivo and in vitro (fig. S7).

Open- or closed-chromatin regions can be indicative of transcriptional regulatory elements and serve as predictors of gene transcription activity. We measured genome-wide chromatin

[1]Department of Microbiology, Immunology, and Molecular Genetics, University of California–Los Angeles, Los Angeles, CA 90095, USA. [2]Division of Hematology and Oncology, Department of Medicine, University of California–Los Angeles, Los Angeles, CA 90095, USA. [3]Department of Molecular and Medical Pharmacology, University of California–Los Angeles, Los Angeles, CA 90095, USA. [4]Department of Ecology and Evolutionary Biology, University of California–Los Angeles, Los Angeles, CA 90095, USA. [5]Department of Biological Chemistry, University of California–Los Angeles, Los Angeles, CA 90095, USA. [6]Department of Pathology, School of Medicine, Duke University, Durham, NC 27710, USA. [7]Molecular Biology Institute, University of California–Los Angeles, Los Angeles, CA 90095, USA. [8]Jonsson Comprehensive Cancer Center, University of California–Los Angeles, Los Angeles, CA 90095, USA. [9]Eli and Edythe Broad Center of Regenerative Medicine and Stem Cell Research, University of California–Los Angeles, Los Angeles, CA 90095, USA. [10]Crump Institute for Molecular Imaging, University of California–Los Angeles, Los Angeles, CA 90095, USA.
*Corresponding author. Email: owenwitte@mednet.ucla.edu (O.N.W.); tgraeber@mednet.ucla.edu (T.G.G.)

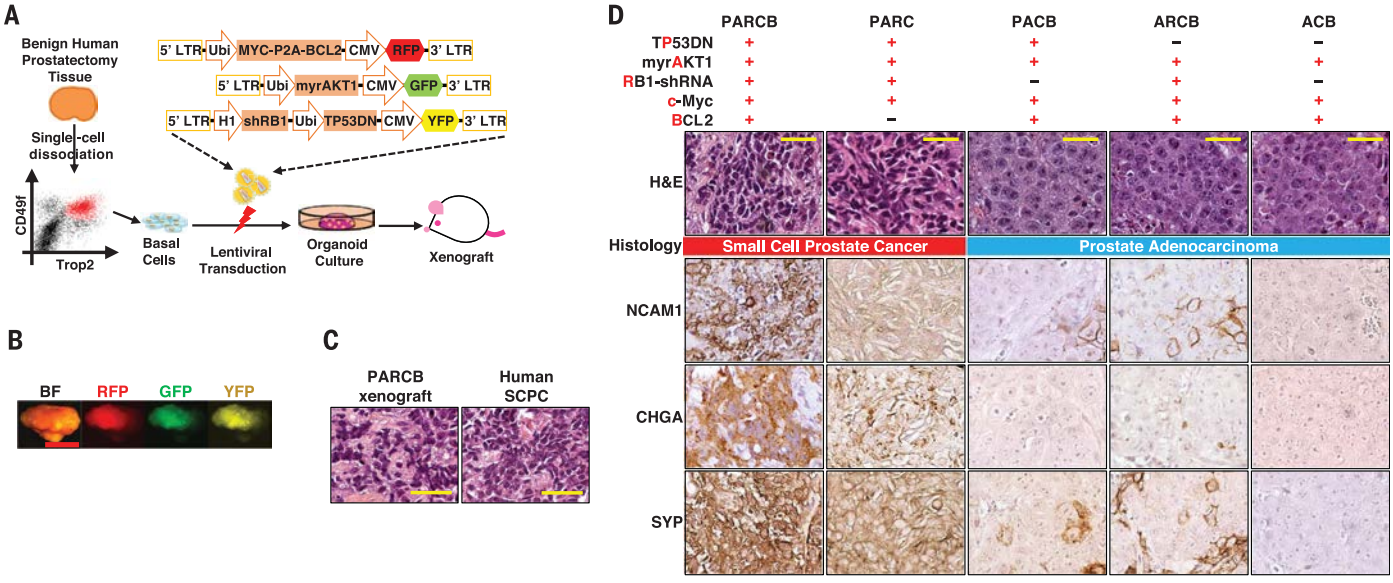

Fig. 1. Defined genes drive human prostate epithelial cells to the SCPC phenotype. (**A**) Schematic of human prostate transformation assay. LTR, long terminal repeats; CMV, cytomegalovirus promoter; Ubi, ubiquitin promoter. (**B**) Representative image of PARCB xenografts displaying GFP, RFP, and YFP expression. BF, bright field. Scale bar, 1 cm. (**C**) Hematoxylin and eosin (H&E)–stained images of PARCB grafts and human SCPC. Scale bars, 50 μm. (**D**) H&E staining and immunohistochemistry (IHC) images with antibodies against the indicated proteins in genetically engineered tumor models. Scale bars, 50 μm.

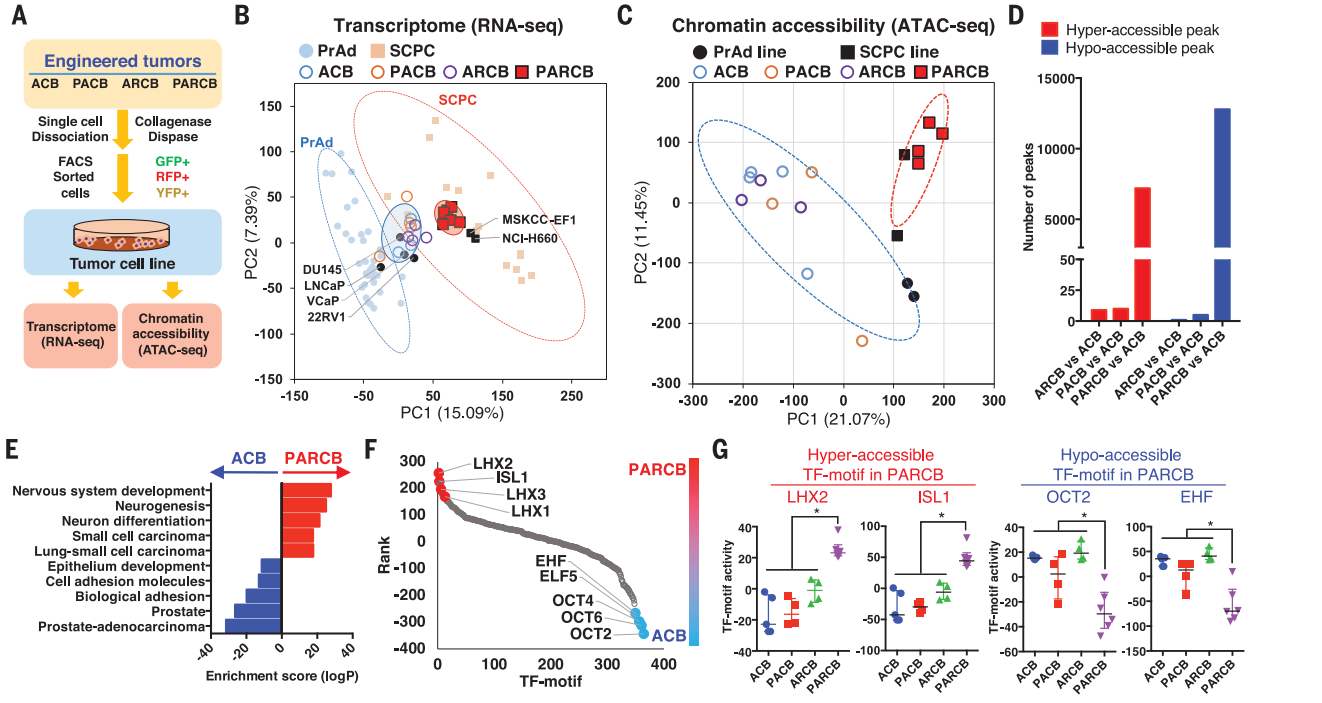

Fig. 2. Inactivation of both p53 and RB is required to reprogram transcriptional profiles and chromatin accessibility landscapes of normal prostate epithelial cells to human SCPC. (**A**) Schematic for establishment of tumor cell lines with GFP-, RFP-, and YFP-positive purified xenograft cells. (**B**) Partial least-squares regression analysis (PLSR) separates PrAd and SCPC specimens in the RNA-seq dataset from Beltran *et al*. (*7*). RNA-seq data for engineered tumor lines and patient-derived prostate cancer cell lines were projected onto the PLSR plot. (**C**) Principal components analysis (PCA) of ATAC-seq data from engineered cell lines with PrAd and SCPC lines. Probability ellipse = 95% confidence to group the samples. (**D**) Hyper- or hypo-accessible peaks in comparisons between engineered tumor lines. (**E**) Selected gene sets enriched in hyper- or hypo-accessible peaks in the comparison between PARCB and ACB lines. (**F**) TF binding motifs identified by HOMER (*34*) motif analysis were plotted by ranks generated from their associated differential adjusted *P* values. (**G**) Transcriptional activities of the TF motifs were measured by gene signature scores (see materials and methods). Medians with interquartile ranges are shown. **P* < 0.05 [one-way analysis of variance (ANOVA)].

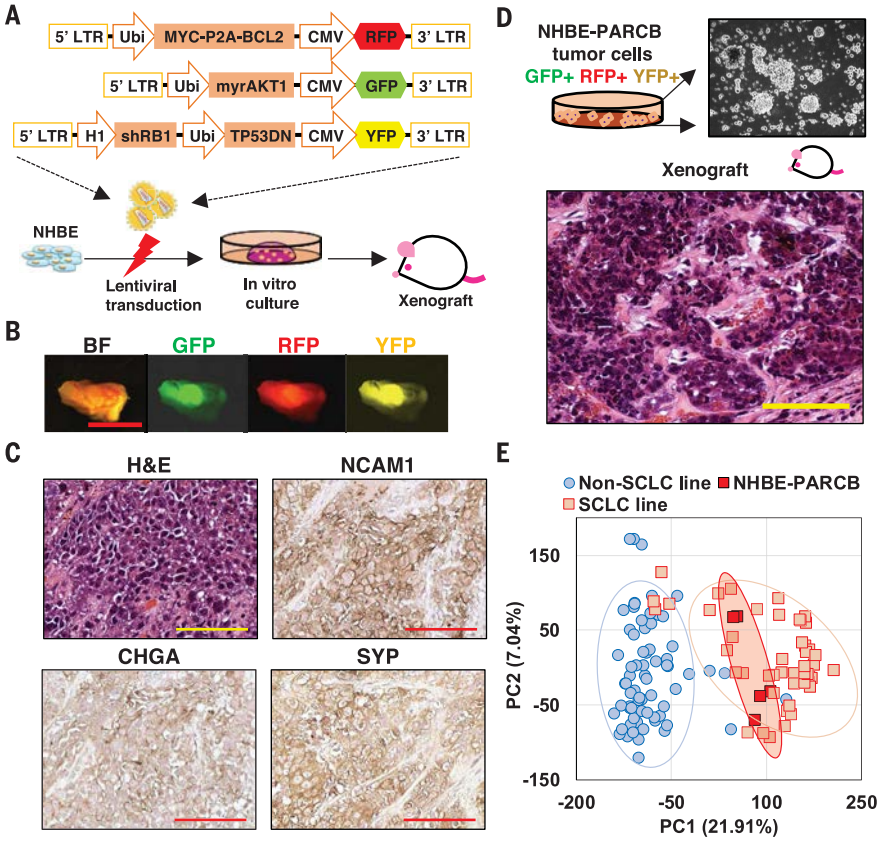

Fig. 3. The same genetic drivers for SCPC can initiate SCLC from human normal lung epithelial cells. (**A**) Schematic of NHBE cell transformation. (**B**) Representative tumor image displaying the lentivirally colinked markers GFP, RFP, and YFP. Scale bar, 1 cm. (**C**) H&E and IHC images against NED markers in transformed NHBE xenografts. Scale bars, 100 μm. (**D**) Representative morphologic image of NHBE-PARCB cell lines in two-dimensional culture and H&E image of xenografts derived from NHBE-PARCB cell lines. Scale bar, 100 μm. (**E**) PCA of NHBE-PARCB cell lines with SCLC and non-SCLC cell lines.

accessibility and its association with transcriptional programs by ATAC-seq. PARCB and patient-derived SCPC lines exhibited a distinct chromatin accessibility status compared with the ACB, PACB, or ARCB lines (Fig. 2C and fig. S4B). Dual inactivation of p53 and RB in PARCB lines induced marked changes in chromatin accessibility compared with that in ACB lines (Fig. 2D). However, single inactivation of p53 or RB alone in PACB or ARCB lines, respectively, did not alter chromatin accessibility compared with that in ACB lines (Fig. 2D).

Chromatin regions in PARCB lines that were hyperaccessible compared with those in ACB lines were highly enriched for genes associated with neuronal differentiation and small cell lung cancer (SCLC), whereas hypo-accessible regions in PARCB lines were enriched for epithelial development– and PrAd-associated genes (Fig. 2E). We conclude that concomitant p53 and RB disruption is required and may synergize to promote lineage plasticity during human prostate epithelial transformation by modulating transcriptional and epigenetic programs, supporting previous findings from mouse models (*8*, *19*).

To further characterize p53 and RB inactivation–induced changes in chromatin, we performed transcription factor (TF) binding motif enrichment analysis with the differentially accessible peaks in PARCB lines compared with ACB lines. We found that LHX family TF motifs (LHX1, LHX2, and LHX3) and ISL1 were the most accessible regions in PARCB lines, whereas OCT family TF motifs (OCT2 and OCT6) and ETS family TF motifs (EHF and ELF5) were less accessible in PARCB than in ACB lines (Fig. 2F and table S1). Although the biological functions of these TFs are unexplored in prostate cancer, we were able to assess the transcriptional activity of these TF motifs altered by concomitant p53 and RB disruption. Our integrated analysis with the matched RNA-seq data revealed that enriched accessibility of LHX2-, ISL1-, OCT2-, or EHF-DNA binding motifs was mirrored by the expression of the downstream target genes (Fig. 2G).

We next investigated how similar the PARCB lines might be to SCNCs from other organs. We performed a gene list enrichment analysis (*20*) of 938 transcriptionally profiled cancer cell lines by using genes up-regulated in the PARCB lines (table S2). This analysis demonstrated that the PARCB cell lines were transcriptionally most similar to SCLC cell lines and the NCI-H660 SCPC cell line (fig. S8 and table S3). To further evaluate the similarity of SCPC and SCLC, we projected gene expression data from human lung cancer samples [from (*21*) and The Cancer Genome Atlas (TCGA) (*22*)] onto our prostate cancer clustering plot in Fig. 2B. All clinical SCLC samples tightly clustered with the SCPC samples, indicating that prostate and lung SCNCs are both histologically and transcriptionally similar (fig. S9).

Given the similarity of the PARCB prostate cancer models to SCPC and SCLC, we next asked whether the PARCB factors could initiate SCLC from human lung epithelial cells. In a fashion similar to our transformation of primary human prostate cells, we transformed primary normal human bronchial epithelial (NHBE) cells with the PARCB lentiviruses (Fig. 3A). Xenografts (NHBE-PARCB) expressed GFP, RFP, and YFP (Fig. 3B) and the PARCB factors (fig. S10A). NHBE-PARCB tumors showed typical histological features and NED marker expression characteristic of clinical SCLC (Fig. 3C). Removing one gene from the PARCB combination did not result in tumor growth. Similar to clinical SCLC (*23*), all of the tumors expressed the proliferation marker Ki67 and none expressed the basal-squamous epithelial cell markers p63 and cytokeratin 14 (fig. S10B).

To interrogate the convergent evolutionary pattern of SCNCs, we established five NHBE-PARCB tumor cell lines for downstream multi-omics analyses. Like the prostate PARCB lines, the NHBE-PARCB lines propagated in suspension, demonstrated tumorigenic potential in vivo (Fig. 3D), and exhibited transcriptional similarity to patient-derived SCLC cell lines [from the Cancer Cell Line Encyclopedia database (*24*)] (Fig. 3E). Comparative genomic hybridization and whole-exome sequencing analyses identified no recurrent genetic alterations between prostate and lung PARCB models, indicating that the defined five genetic factors are likely sufficient to drive human SCNC (fig. S11 and tables S4 and S5).

We found that normal prostate basal epithelial cells and NHBE cells displayed distinct transcriptomes. In contrast, the prostate PARCB and NHBE-PARCB cell lines tightly clustered together, indicating a shared gene expression profile associated with reprogramming by the PARCB factors irrespective of the tissue of origin (Fig. 4A). We then examined transcriptome data from SCPC and SCLC patient biopsy specimens (*7*, *21*) and compared these with their respective adjacent normal tissues from TCGA. These results support the finding that SCPC and SCLC are transcriptionally convergent relative to the normal epithelial cells from which they originated (Fig. 4B) and demonstrate that a similar convergence occurs in patients.

Both transcriptional and epigenetic regulatory networks dictate cell lineage decisions (*25*, *26*). We investigated the nature of the global chromatin states involved in the convergent transformation to SCNC by ATAC-seq. PARCB, SCPC,

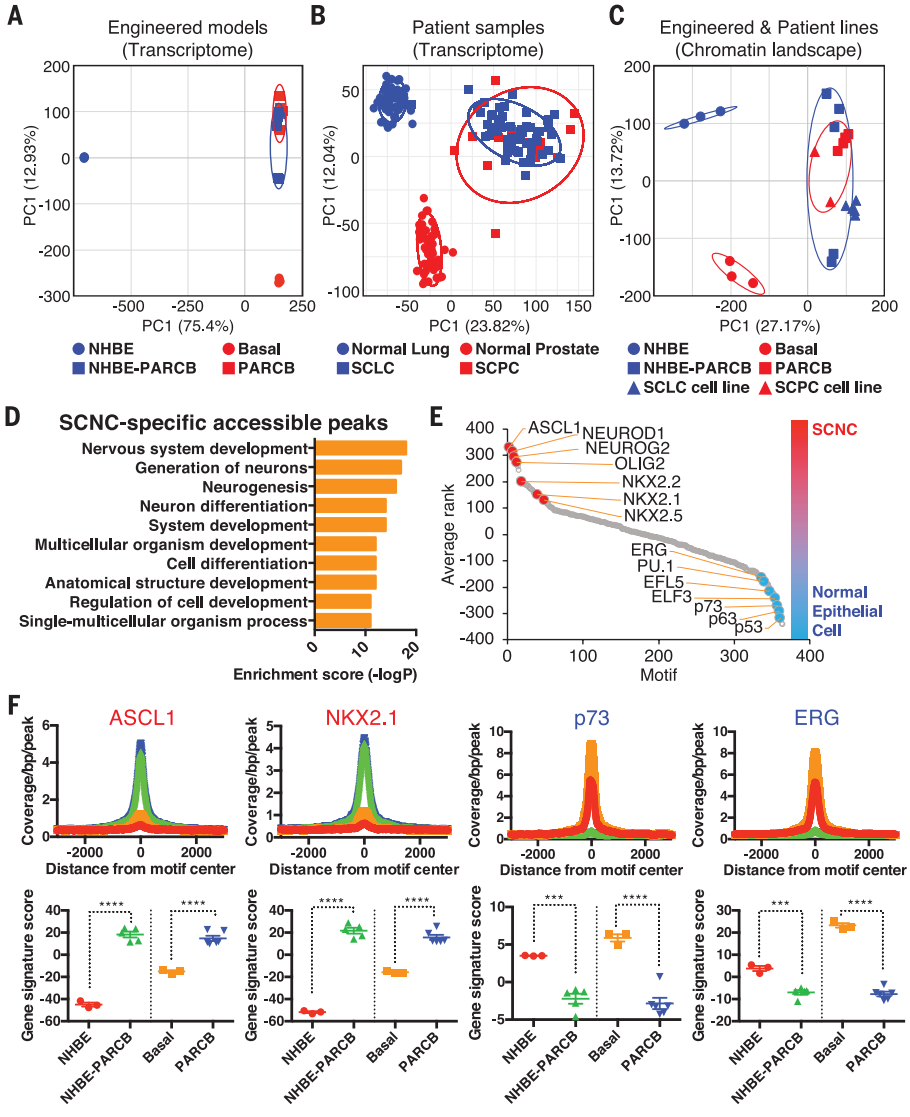

Fig. 4. Convergent transcriptional and chromatin accessibility landscapes of SCPC and SCLC identify shared TF motifs. (**A**) PCA of RNA-seq data from normal lung and prostate epithelial cells (NHBE and basal) and engineered lung and prostate PARCB cells. (**B**) PCA of RNA-seq data from human samples: SCLC and SCPC specimens and adjacent normal lung and prostate tissues. (**C**) PCA of ATAC-seq data from NHBE, basal, NHBE-PARCB, PARCB, and patient-derived SCLC and SCPC lines. (**D**) Gene Ontology terms for hyperaccessible peaks in lung and prostate SCNCs. (**E**) TF motifs identified by HOMER motif analysis were plotted by ranks generated from their associated differential *P* values (table S7). (**F**) (Top) Selected visualization of ATAC-seq footprint. bp, base pair. (Bottom) The transcriptional activities were measured by gene signature scores (see materials and methods). Medians with interquartile ranges are shown. ***$P < 0.001$, ****$P < 0.0001$ (one-way ANOVA).

and SCLC lines exhibited similar chromatin accessibility landscapes (Fig. 4C and fig. S12), which paralleled their transcriptional resemblance. Notably, the chromatin accessibility profiles of patient-derived SCPC and SCLC cell lines clustered with our prostate and NHBE-PARCB cell lines but not with non-neuroendocrine prostate and lung epithelial cells (Fig. 4C). We identified shared hyper- and hypo-accessible chromatin regions in the lung and prostate SCNCs compared with normal lung and prostate epithelial cells (fig. S13). The SCNC-specific accessible regions were enriched for genes important for development and neuronal differentiation (Fig. 4D and table S6).

To gain insight into the possible biological roles of TFs that serve as master regulators in SCNCs, we performed DNA binding motif enrichment analysis of the hyperaccessible regions. This analysis revealed motifs corresponding to proneural TFs (ASCL1, NEUROD1, NEUROG2, and OLIG2) and NKX homeodomain TFs (NKX2.1, NKX2.2, NKX2.5, and NKX6.1) (Fig. 4E and table S7). ASCL1 and NEUROD1 are required for SCLC survival and initiation (*27*–*29*). NEUROD1, NEUROG2, and NKX homedomain TFs are implicated in neural stem cell patterning and neural progenitor fate specification (*30*). NKX2.1/TTF-1 is a biomarker for SCLC and SCPC (*31*). We found that the chromatin regions for binding p53 family TFs (p53, p63, and p73) and ETS family TFs (ELF3, ELF5, and ERG) were less accessible in SCNCs than in normal epithelial cells (Fig. 4E). Both of these TF families also play critical roles in neuronal development and lineage decisions (*32*, *33*). Our motif analysis identified TFs known to be involved in neural proliferation and differentiation as well as additional TFs (table S7) with unexplored roles in SCNC. We next evaluated both RNA-seq and ATAC-seq data to compare the transcriptional activity of these TFs with the global accessibility of their DNA binding motifs. Our integrated analysis revealed that the differentially accessible TF motifs we identified correlated with the transcriptional output of TF target genes for each motif (Fig. 4F and fig. S14). These findings indicate that concomitant enrichment of proneural TFs and NKX homeodomain TFs and silencing of ETS family TF and p53 family TF transcriptional activities are conserved in and are likely critical for transformation to SCNC across tissue types.

Current therapeutic strategies designed to inhibit oncogenic pathways driving malignant phenotypes almost inevitably lead to treatment-resistant cancers. Increasingly, treatment-resistant tumors that assume aggressive clinical characteristics and molecular features of both stemlike and neuroendocrine lineages are being identified in a variety of epithelial cancers. We provide cellular, transcriptional, and epigenetic evidence that the SCNC phenotype that arises from distinct epithelial organs represents a common point in the evolution of cancers that is induced by shared genetic and epigenetic processes. Although normal human epithelial cells derived from developmentally distinct organs have their own molecular landscapes, our findings demonstrate that a defined set of oncogenic factors can induce the development of a common lethal neuroendocrine cancer lineage (SCNC) from different epithelial cell types. We have characterized the essential contribution of these factors and the convergence of both the transcriptional and chromatin landscapes during the process of transformation to SCNC. Our integrated molecular analyses have identified a group of key TFs that appear to be critical for the initiation and maintenance of SCNC, independently of the tissue of origin. These data may help inform efforts to identify novel therapeutic approaches for preventing the emergence of SCNCs and for treating them once they arise.

REFERENCES AND NOTES

1. D. Hanahan, R. A. Weinberg, *Cell* **144**, 646–674 (2011).
2. R. Nadal, M. Schweizer, O. N. Kryvenko, J. I. Epstein, M. A. Eisenberger, *Nat. Rev. Urol.* **11**, 213–219 (2014).
3. A. F. Gazdar, P. A. Bunn, J. D. Minna, *Nat. Rev. Cancer* **17**, 765 (2017).
4. L. V. Sequist *et al.*, *Sci. Transl. Med.* **3**, 75ra26 (2011).
5. H. L. Tan *et al.*, *Clin. Cancer Res.* **20**, 890–903 (2014).

6. M. J. Niederst *et al*., *Nat. Commun.* **6**, 6377 (2015).
7. H. Beltran *et al*., *Nat. Med.* **22**, 298–305 (2016).
8. S. Y. Ku *et al*., *Science* **355**, 78–83 (2017).
9. R. Fisher *et al*., *Genome Biol.* **15**, 433 (2014).
10. H. Chen, X. He, *Mol. Biol. Evol.* **33**, 4–12 (2016).
11. N. McGranahan, C. Swanton, *Cell* **168**, 613–628 (2017).
12. T. Stoyanova *et al*., *Proc. Natl. Acad. Sci. U.S.A.* **110**, 20111–20116 (2013).
13. V. Parimi, R. Goyal, K. Poropatich, X. J. Yang, *Am. J. Clin. Exp. Urol.* **2**, 273–285 (2014).
14. J. K. Lee *et al*., *Cancer Cell* **29**, 536–547 (2016).
15. Y. Lin, J. Fukuchi, R. A. Hiipakka, J. M. Kokontis, J. Xiang, *Cell Res.* **17**, 531–536 (2007).
16. M. Krajewska *et al*., *Am. J. Pathol.* **148**, 1567–1576 (1996).
17. L. D. Shultz, F. Ishikawa, D. L. Greiner, *Nat. Rev. Immunol.* **7**, 118–130 (2007).
18. P. Mu *et al*., *Science* **355**, 84–88 (2017).
19. M. Zou *et al*., *Cancer Discov.* **7**, 736–749 (2017).
20. E. Y. Chen *et al*., *BMC Bioinformatics* **14**, 128 (2013).
21. J. George *et al*., *Nature* **524**, 47–53 (2015).
22. National Cancer Institute, The Cancer Genome Atlas; https://cancergenome.nih.gov/.
23. H. Zhang *et al*., *Mod. Pathol.* **18**, 111–118 (2005).
24. J. Barretina *et al*., *Nature* **483**, 603–607 (2012).
25. W. K. Cheung, D. X. Nguyen, *Oncogene* **34**, 5771–5780 (2015).
26. W. A. Whyte *et al*., *Cell* **153**, 307–319 (2013).
27. H. Osada, Y. Tatematsu, Y. Yatabe, Y. Horio, T. Takahashi, *Cancer Res.* **65**, 10680–10685 (2005).
28. T. Jiang *et al*., *Cancer Res.* **69**, 845–854 (2009).
29. J. K. Osborne *et al*., *Proc. Natl. Acad. Sci. U.S.A.* **110**, 6524–6529 (2013).
30. F. Guillemot, *Development* **134**, 3771–3780 (2007).
31. S. N. Agoff *et al*., *Mod. Pathol.* **13**, 238–242 (2000).
32. P. Remy, M. Baltzinger, *Oncogene* **19**, 6417–6431 (2000).
33. B.Joseph, O. Hermanson, *Exp. Cell Res.* **316**, 1415–1421 (2010).
34. S. Heinz *et al*., *Mol. Cell* **38**, 576–589 (2010).

ACKNOWLEDGMENTS

We thank the University of California, Los Angeles (UCLA) Tissue Procurement Core Laboratories for tissue preparation and the UCLA Technology Center for Genomics and Bioinformatics for preparing for RNA-seq and ATAC-seq analyses. We thank Y. Chen at Memorial Sloan Kettering Cancer Center for sharing the MSK-PCa4 SCPC organoid cell line. **Funding:** J.W.P. is supported by a UCLA Broad Stem Cell Research Center postdoctoral fellowship and the National Institutes of Health/National Cancer Institute (NIH/NCI) grant K99/R00 Pathway to Independence award K99CA218731. J.K.L. is supported by a Prostate Cancer Foundation (PCF) Young Investigator award and a Department of Defense (DOD) Prostate Cancer Research Program-Physician Research award. B.A.S. is supported by a PCF Young Investigator award and an American Cancer Society postdoctoral fellowship award. K.M.S. is supported by the UCLA Medical Scientist Training Program (NIH NIGMS T32 GM008042). C.C. and S.K.K. are supported by NIH grant CA178415. J.H. is supported by National Cancer Institute grants 1R01CA172603-01A1 and 1R01CA205001-01. T.G.G. is supported by the NCI/NIH (P01 CA168585) and an American Cancer Society Research Scholar award (RSG-12-257-01-TBE). T.G.G. and O.N.W. are supported by the UCLA SPORE in Prostate Cancer (NIH P50 CA092131) and a grant from the Medical Research Grant Program of the W. M. Keck Foundation. O.N.W. is supported by the Eli and Edythe Broad Center of Regenerative Medicine and Stem Cell Research and the Hal Gaba Fund for Prostate Cancer Research. **Author contributions:** J.W.P., J.K.L., B.A.S., and O.N.W. designed the study and experiments. J.W.P., J.K.L., L.W., and K.N. prepared lentiviral constructs, performed human prostate and lung transformation assays, and prepared samples for RNA-seq and ATAC-seq. J.W.P., L.W., and K.N. performed immunostaining analyses. J.W.P., N.G.B., K.M.S., B.A.S., C.C., B.L.T., S.K.K., and T.G.G. contributed to designing and performed bioinformatics analyses with RNA-seq and ATAC-seq data. S.K.K. and T.G.G. supervised the bioinformatics analyses. D.C. and K.N. contributed to processing human tissues and performing FACS analysis. J.H., L.W., and K.N. performed histological analyses. O.N.W. supervised the research. J.W.P. and O.N.W. wrote the manuscript with input from all authors. **Competing interests:** O.N.W. is a Scientific Advisor for Kronos Bio, a company developing chemical modulators of TFs and other targets in oncology. **Data and materials availability:** The RNA-seq, ATAC-seq, and whole-exome shotgun sequencing data reported in this article have been deposited in NCBI GEO under accession number GSE118207.

SUPPLEMENTARY MATERIALS

www.sciencemag.org/content/362/6410/91/suppl/DC1
Materials and Methods
Figs. S1 to S14
Tables S1 to S11
References (*35*–*50*)

14 March 2018; resubmitted 3 July 2018
Accepted 9 August 2018
10.1126/science.aat5749

Science

Reprogramming normal human epithelial tissues to a common, lethal neuroendocrine cancer lineage

Jung Wook Park, John K. Lee, Katherine M. Sheu, Liang Wang, Nikolas G. Balanis, Kim Nguyen, Bryan A. Smith, Chen Cheng, Brandon L. Tsai, Donghui Cheng, Jiaoti Huang, Siavash K. Kurdistani, Thomas G. Graeber and Owen N. Witte

Science **362** (6410), 91-95.
DOI: 10.1126/science.aat5749

Some (re)programming notes on cancer

Epithelial cancers develop resistance to targeted therapies in a number of different ways. Several cancer types do so by undergoing phenotypic conversion to a highly aggressive cancer called small cell neuroendocrine carcinoma (SCNC). Whether distinct cancer types accomplish this "reprogramming" through the same mechanism has been unclear. Park *et al.* show that the same set of oncogenic factors transforms both normal lung and normal prostate epithelial cells into SCNCs that resemble clinical samples (see the Perspective by Kareta and Sage). This convergence of molecular pathways could potentially simplify the development of new therapies for SCNC, which is currently untreatable.

Science, this issue p. 91; see also p. 30

Supplementary Materials for

Reprogramming normal human epithelial tissues to a common, lethal neuroendocrine cancer lineage

Jung Wook Park, John K. Lee, Katherine M. Sheu, Liang Wang, Nikolas G. Balanis, Kim Nguyen, Bryan A. Smith, Chen Cheng, Brandon L. Tsai, Donghui Cheng, Jiaoti Huang, Siavash K. Kurdistani, Thomas G. Graeber*, Owen N. Witte*

*Corresponding author. Email: owenwitte@mednet.ucla.edu (O.N.W.); tgraeber@mednet.ucla.edu (T.G.G.)

Published 5 October 2018, *Science* **362**, 91 (2018)
DOI: 10.1126/science.aat5749

This PDF file includes:

Other Supplementary Material for this manuscript includes the following:
(available at www.sciencemag.org/content/362/6410/91/suppl/DC1)

Materials and Methods

Lentiviral Vectors and lentiviruses

The myristoylated AKT1 vector (FU-myrAKT1-CGW) has been described previously (*35*). For cloning of the c-MYC-P2A-BCL2 vector, P2A-BCL2 cDNA (BC027258.1) oligo (Integrated DNA Technologies, IDT) was added to our c-Myc lentiviral backbone vector (FU-MYC-CRW) (*12*) using Gibson-assembly master mix (NEB, CAT# E2611). For cloning of the vector expressing shRNA for knocking down RB1 and dominant negative TP53 (R175H), cDNA of dominant negative TP53 mutant (R175H) was obtained from Addgene (plasmid# 16436). H1-promoter-RB1shRNA oligo purchased from IDT (shRNA targeting 3'UTR: CCGGCAGAGATCGTGTATTGAGATTCTCGAGAATCTCAATACACGATCTCTGTTTTT from TRCN0000295842 and (*36*)). These two inserts were added by this order (H1 promoter-RB1-shRNA and ubiquitin promoter-TP53DN) to FU-CYW lentiviral vector (CYW=CMV promoter-YFP Woodchuck hepatitis virus posttranscriptional regulatory element). The resulting plasmids are now described as FU-MYC-P2A-BCL2-CRW and FU-RB1-shRNA-TP53DN-CYW with construct design presented in Fig. 1A. Lentiviruses were produced and purified by a previously described method (*37*).

Human prostate tissues and organoid transformation assay

Donor tissues were provided in a de-identified manner and thus were exempt from Institutional Review Board (IRB) approval. Acquisition and processing of human tissue, dissociation and isolation of distinct epithelial subsets, and lentiviral transduction have been described in detail previously (*38*). FACS-isolated cells (10,000-20,000 cells/organoid graft) were plated in 20-30μL of growth factor-reduced Matrigel (Corning, CAT# 356234) with lentiviruses (MOI=50/lentivirus). Organoid culture was performed as described previously (*39*). After 1-2 week culture, transduced organoids were harvested by dissociation of Matrigel with 1mg/mL Dispase (Thermo Fisher Scientific, CAT# 17105041). The organoids were washed three times with PBS to remove Dispase and re-suspended in 20-30μl of Matrigel. The organoid-Matrigel mixture was implanted subcutaneously in immunodeficient NOD.Cg-*Prkdcscid Il2rgtm1Wjl*/SzJ (NSG) (*17*) mice using a 28-gauge syringe. Xenografts were harvested within 2-3 months or when they reached 1cm big in their diameter.

Animal and Subcutaneous transplantation

For xenograft analysis, NSG mice had been transferred from the Jackson Laboratories and housed and bred under the care of the Division of Laboratory Animal Medicine at the University of California, Los Angeles (UCLA). Subcutaneous injection of cells was performed according to protocols approved by UCLA's Animal Research Committee.

Tissue section and Histology

Tumor tissues were pre-fixed in 10% buffered formaldehyde for overnight at 4°C, then moved into 70% ethanol. They were embedded in paraffin and sectioned at 5 μm at the Translational Pathology Core Laboratory (TPCL) where is a CAP/CLIA certified research facility in the UCLA Department of Pathology and Laboratory Medicine and a UCLA Jonsson Comprehensive Cancer Center Shared Facility. Every 5th section was stained for hematoxylin and eosin (H&E) for histology. The histology was blindly evaluated/graded by multiple pathologists in UCLA.

Immunostaining

For the immunohistochemistry (IHC) staining on formalin-fixed paraffin embedded sections, 5 μm sections were deparaffinized and rehydrated. Citrate buffer (pH 6.0) was used for antigen retrieval. The sections were heated in citrate buffer for 30 min in a pressure cooker using microwave. Endogenous peroxidase activity was blocked by 3% H_2O_2 in methanol for 10 min at room temperature. Primary antibodies were incubated overnight at 4°C. Anti-mouse/rabbit biotinylated secondary antibodies were used to detect proteins. ImmPACT DAB (Vector laboratories, CAT# SK-4105) was used as described in their protocol to visualize the staining. Slides were dehydrated and mounted.

For the western blot analysis, protein was extracted from tumors and cell lines using UREA buffer (8M UREA, 4% CHAPS, 1X protease inhibitor cocktail (Roche, CAT# 11697498001), and 1X phosphatase inhibitor cocktail (Cell Signaling Technology, CAT# 5870)). Genomic DNA was removed by an ultracentrifuge (Beckman Optima MAX-XP, 45,000RPM). The concentration of total protein was measured by BCA analysis (Pierce, CAT# 23225). Western blots were visualized by using a film developer.

Each immunostaining was independently performed more than two times.

Antibodies

Antibodies used for flow cytometry included CD49f-PE (12-0495-82; eBiosciences), HLA-A/B/C-biotin (565291; BS Bioscience), and Trop2-APC (FAB650A; R&D Systems). Antibodies used for IHC and western blots included cytokeratin 14 (PRB-155P; Covance), p63 and AR (SC-8431 and SC-816; Santa Cruz Biotechnology), c-Myc (ab32072, Abcam), p-AKT (9271; Cell Signaling), Ki67 (ab16667; Abcam), BCL2 (ab32124; Abcam), p53 (2527, Cell Signaling Technology), RB (ab181616; Abcam), GAPDH (GTX627408-01; Genetex), SYP (M7315; Dako), NCAM1/CD56 (ab75813; Abcam), and CHGA (M869; Dako).

Cell lines

LNCaP (CRL-1740), 22RV1 (CRL-2505), NCI-H660 (CRL-5813), NCI-H524 (CRL-5831), NCI-H1436 (CRL-5871), NCI-H1963 (CRL-5982), NCI-H2171 (CRL-5929), and NCI-H2227 (CRL-5934) cells were obtained from American Type Culture Collection (ATCC) and maintained as recommended by ATCC. Cell line authentication was confirmed by STR (Short Tandem Repeat) by using Promega PowerPlex16 HS kit (performed by Laragen). MSKCC-EF1 cells; we obtained MSK-PCa4 organoid cell line described previously (*40*) from Dr. Yu Chen in MSKCC and cultured them in 2D culture using stem cell culture media (Advanced DMEM/F12 (Gibco CAT# 12634028), Glutamax (Gibco, CAT# 35050061), B27 (Gibco CAT# 17504044, 10ng/ml human EGF (Peprotech CAT# 100-47, and 10ng/ml human FGF-basic (Peprotech CAT# 100-18B)). We named it MSKCC-EF1 cell line to distinguish its parental organoid cell line. MSKCC-EF1 cell line expresses NED markers (Synaptophysin, NCAM1/CD56, and Chromogranin A) *in vitro* and is tumorigenic *in vivo*. Primary NHBE cell lines (*41*) were purchased from Lonza (CC-2540) and were utilized for our lung transformation assay. All NHBEs did not come from donors with airway-related diseases (Lonza). They were maintained and passaged as described on Lonza's website (www.lonza.com). All NHBE cells were used for our transformation assay before they reached passage 7. Our genetically engineered tumor cell lines of the prostate and lung were maintained in the stem cell culture media. The PARCB lines grow in suspension as floating clusters (fig. S7A), consistent with patient-derived small cell lung and prostate cancer lines (*42, 43*). Their double times are between 20-24 hours.

STR analysis was performed following ANSI/ATCC ASN-0002-2011 procedure to show human origin and authenticate our genetically engineered human small cell cancer lines (table S8). We calculated matched allele percentages between the samples using data from STR analysis (table S8). Six human prostate and three human lung materials were utilized in this study for our transformation assay (NHBE1-PARCB-1, NHBE1-PARCB-2, NHBE4-PARCB-1, and NHBE4-PARCB-2 cell lines are derived from NHBE1 and NHBE4 cells, respectively). All the cell lines in the study are Mycoplasma free, which is tested by MycoAlert™ PLUS Mycoplasma Detection Kit (Lonza, cat# LT07-703).

RNA-sequencing (RNA-seq)

For RNA-seq, library preparation and sequencing were performed by the Technology Center for Genomics & Bioinformatics (TCGB) at UCLA. Libraries for RNA-seq were prepared with KAPA Stranded RNA-seq Kit. The workflow consists of mRNA enrichment, cDNA generation, and end repair to generate blunt ends, A-tailing, adaptor ligation and PCR amplification. Different adaptors were used for multiplexing samples in one lane. Sequencing was performed on Illumina HiSeq 3000 for a pair read 150 base run. Data quality check was done on Illumina SAV. Demultiplexing was performed with Illumina Bcl2fastq2 v 2.17 program. FASTQ files were processed using the TOIL processing pipeline (https://github.com/BD2KGenomics/toil-rnaseq), RNAseq measurements were expressed as upper quartile normalized counts. Data were log2 transformed and filtered for coding genes using HUGO (http://www.genenames.org/). The reads were aligned to the hg38 human genome. The details of the RNA-seq data are described in table S9.

Gene expression datasets of CCLE lung cancer cell lines

Gene expression data of CCLE lung cancer cell lines were obtained as FASTQ files and were converted from bam files back to FASTQs using Picard tools (https://broadinstitute.github.io/picard/) and Sambamba (http://lomereiter.github.io/sambamba/). FASTQ files were processed using the TOIL processing pipeline, RNA-seq measurements are expressed as upper quartile normalized counts. Data were log2 transformed and filtered for coding genes using HUGO (http://www.genenames.org/).

Computational analyses (PCA and PSLR analysis)

Principle component analysis (PCA) is an unsupervised learning approach that decomposes a matrix X into orthogonal principal components that maximize the variance explained in X. Partial least squares regression analysis (PLSR) (*44*) is a supervised learning approach that decomposes a matrix X of predictors and dependent variables Y into orthogonal components while also maximizing the *covarianc*e between the two matrices. In our analysis data, the X matrix is the RNA-seq expression matrix of human patient data (*7*) and the Y matrix is a binary vector on the PrAd/SCPC classification (table S10). Projections onto this PLSR space were performed with our human cell line model systems. All analyses were performed on mean centered data.

Library preparation of ATAC-sequencing (ATAC-seq)

Libraries for ATAC-seq were prepared by a previously described method (*45*). Eight different indexes were used for multiplexing samples in each sequencing (*45*). Sequencing was performed on illumine HiSeq 2000 for a single read 50 base run. Data were processed with

ENCODE pipeline (https://www.encodeproject.org/atac-seq). Each sample obtained at least 50M mapped reads for following analyses. Data were deposited into GEO database and the details were described in table S11.

ATAC-seq analysis

Raw files (fastq format) processed through the ATAC-seq pipeline published by ENCODE (https://github.com/kundajelab/atac_dnase_pipelines). Briefly, reads were trimmed, filtered, and aligned to hg38. MACS2 was used to call peaks for each individual sample. The Irreproducible Discovery Rate (IDR) peak output from the ENCODE unreplicated-sample ATAC-seq pipeline was used for downstream analysis. IDR measures the reproducibility of peak calls on replicates or pseudo-replicates and uses that score to determine the cutoff for significant peaks. The threshold P-value used was 0.05. Other ENCODE3 parameters were enforced with the flag-encode3. Reads that mapped to mitochondrial genes or blacklisted regions, as defined by the ENCODE pipeline, were removed. Peak files were merged using bedtools merge to obtain a consensus set of peaks across samples. The number of reads that fell into the peaks was obtained using bedtools multicov (*46*), with parameters -q30 to exclude reads with poor mapping quality, and -f 0.05 to exclude reads that only minimally overlap the peak. DESeq2 (*47*) was used for normalizing read counts and determining hyper- and hypo-accessible peaks across normal and SCNC samples, using default parameters and without independent filtering or Cook's cutoff. Peaks were called as hyper or hypo-accessible using abs (log2 fold change)>0.5 and adjusted $P<0.05$.

Prostate model analysis

Comparison of PARCB, ARCB, PACB, and ACB samples was performed using a consensus peak set of peaks merged across these samples. Raw count normalization and analysis of differential peaks between each combination of two groups was performed using DESeq2 as described above. ARCB vs. ACB and PACB vs. ACB comparisons yielded very few significantly differential peaks using the pre-ascertained cutoffs. Motif analysis was then run separately on hyper- or hypo-accessible peaks in the PARCB vs. ACB comparison using HOMER (*34*), with the flags -size 200 and -mask. Motifs specific to hyper or hypo accessible peaks were obtained by taking the rank difference of the motifs in the two lists. To obtain gene expression signatures for genes associated with each motif, the motifs were matched to differentially accessible peaks in the PARCB vs. ACB comparison. Motifs were associated with a peak if they were +/-50bp from the peak center, and peaks were mapped to genes if within +/-1000bp of the transcription start site (TSS). For each motif of interest, the expression values for the motif-associated genes were then converted to z-score across all engineered cell line samples, and the sum z-score was calculated.

Lung and prostate analysis

Analysis of lung and prostate normal epithelial and PARCB samples was performed by merging peaks across these samples. Normal epithelial cell vs. PARCB tumor cell samples were then compared separately for lung and prostate. Significance of overlap for hyper- and hypo-accessible peaks between lung and prostate tissue was calculated using a hypergeometric p-value, out of a total number of peaks of 84985. Gene ontology and genomic annotations were conducted using HOMER, with default parameters. For PCA on ATAC-seq samples, a variance-stabilizing transformation was performed on the count data.

Motif analysis was done using HOMER against a whole genome background and searching for motifs within +/-100bp from the peak center. All motifs were ranked by p-value separately for lung and prostate tissues and then the ranks for both lung and prostate were averaged to obtain rank lists of hyper or hypo-accessible motifs. For each motif, the difference in rank (hyper-hypo) was plotted on the waterfall plot to identify motifs enriched only in hyper-accessible peaks or only in hypo-accessible peaks. Motifs that fell below $P<0.05$ in both lists were removed. To determine whether differential accessibility corresponded to differential gene expression, peaks were centered on the motif, and peaks were mapped to genes using HOMER, with default parameters. Peaks were mapped to genes if within +/-1000bp of the transcription start site (TSS), and motifs were associated with a peak if they were +/-50bp from the peak center. These motif-associated genes were then converted to z-score across normal and PARCB samples, and for each motif, the sum z-score was calculated. Motif-centered histograms were generated with bins of 5bp using HOMER.

Pan-tissue Analysis

DNase data was obtained by download of filtered bam files from the ENCODE website. Files with extremely low SPOT score or extremely low read depth were excluded. Bedtools multicov was used to obtain the number of reads that fell into the total set of peaks previously compiled from the ATAC-seq analysis, resulting in a common set of features across ATAC and DNase data. The DNase data was then also transformed through a variance-stabilizing transformation using the DESeq2 package. The similarity of each sample to PARCB samples was obtained by first performing PCA on normal and PARCB lung and prostate samples using all peaks, and then projecting the DNase data onto this PCA space. Projections were performed by multiplying the original PCA loadings by the data matrix to be projected.

Unsupervised hierarchical clustering

Hierarchical clustering was performed using the *pheatmap* package in R. All hierarchical clustering was done using the clustering method ward-D2, using Spearman correlation as the distance metric unless otherwise specified, and was performed on all relevant features (for example, all genes for RNA-seq or all peaks for ATAC-seq). All clustering analyses were performed on normalized data.

Androgen receptor (AR)-associated gene signature

To evaluate AR signaling, gene expression-based AR signature scores were calculated using a combined list of genes up-regulated in LNCaP cells in response to synthetic androgen R1881 from two previous publications (*48*, *49*). Genes in the signature were z-scored across primary PrAd, CRPC-PrAd, SCPC, prostate cancer cell lines, and prostate-PARCB cell lines, and sum z-scores for each sample were calculated to obtain the androgen response signature score.

Neuroendocrine signature score

To evaluate the extent of an expression-based neuroendocrine phenotype in the engineered prostate models, signature scores were calculated based on genes from a previous publication of human prostate neuroendocrine tumor biopsies (*7*). Genes in the signature were divided into upregulated genes and downregulated genes. The combined signature score was calculated by adding the sum z-score for upregulated genes with the reversed sum z-score for downregulated genes.

Copy number variation and Whole exome sequencing analysis

Copy number analysis was performed on an Affymetrix Cytoscan HD Array and data was processed using the Affymetrix Chromosome Analysis Suite v3.1.0.15 with the NA33 reference model and using the HighResolution setting. Exomes were isolated with the SeqCap EZ Human Exome Library v3.0 (Roche) and libraries were prepared using the Low-Throughput Library Preparation Kit with standard PCR amplification module (KAPA Biosystems). High-throughput sequencing with 150bp paired-end reads was performed using an Illumina HiSeq3000. Mapping of exome sequencing reads was performed using a computational analysis tool, GATK4 (https://software.broadinstitute.org/gatk/gatk4) with the hg38 reference. As no matched normal samples were available GATK4 was run in Tumor-only mode with default settings and the gnomAD germline reference. The output VCF was filtered for sites where the Variant Allele Frequency (VAF)>0.05, read depth>20, and PHRED base and mapping quality scores (MBQ and MMQ) were above 30, which represents 99.9% accuracy. The VCF was then annotated using ANNOVAR (*50*) and a database of SNP sites (avsnp database, https://www.ncbi.nlm.nih.gov/projects/SNP) and known cancer mutations (https://cancer.sanger.ac.uk/cosmic). Sites are reported if they fall in the COSMIC whitelist and did not appear in the avsnp database.

Captions for Table S1 to S11

Table S1	List of ranked transcription factor motifs in PARCB
Table S2	Upregulated genes in PARCB cell lines compared to patient-derived prostate adenocarcinoma cell lines
Table S3	Human cancer cell lines showing a similar gene list to PARCB cell lines (Gene list enrichment analysis)
Table S4	Gene list from GISTIC analysis of CGH data
Table S5	Mutated genes in PARCB cell lines of the prostate and lung
Table S6	Gene Ontology terms with genes associated with SCNC hyper-accessible peaks
Table S7	List of ranked transcription factor motifs in small cell neuroendocrine carcinoma of the prostate and lung from differential motif accessibility analysis
Table S8	Percentage of matched STR between engineered PARCB cell lines
Table S9	RNA-seq sequencing stats
Table S10	List of weighted genes for PLSR plot
Table S11	ATAC-seq sequencing stats

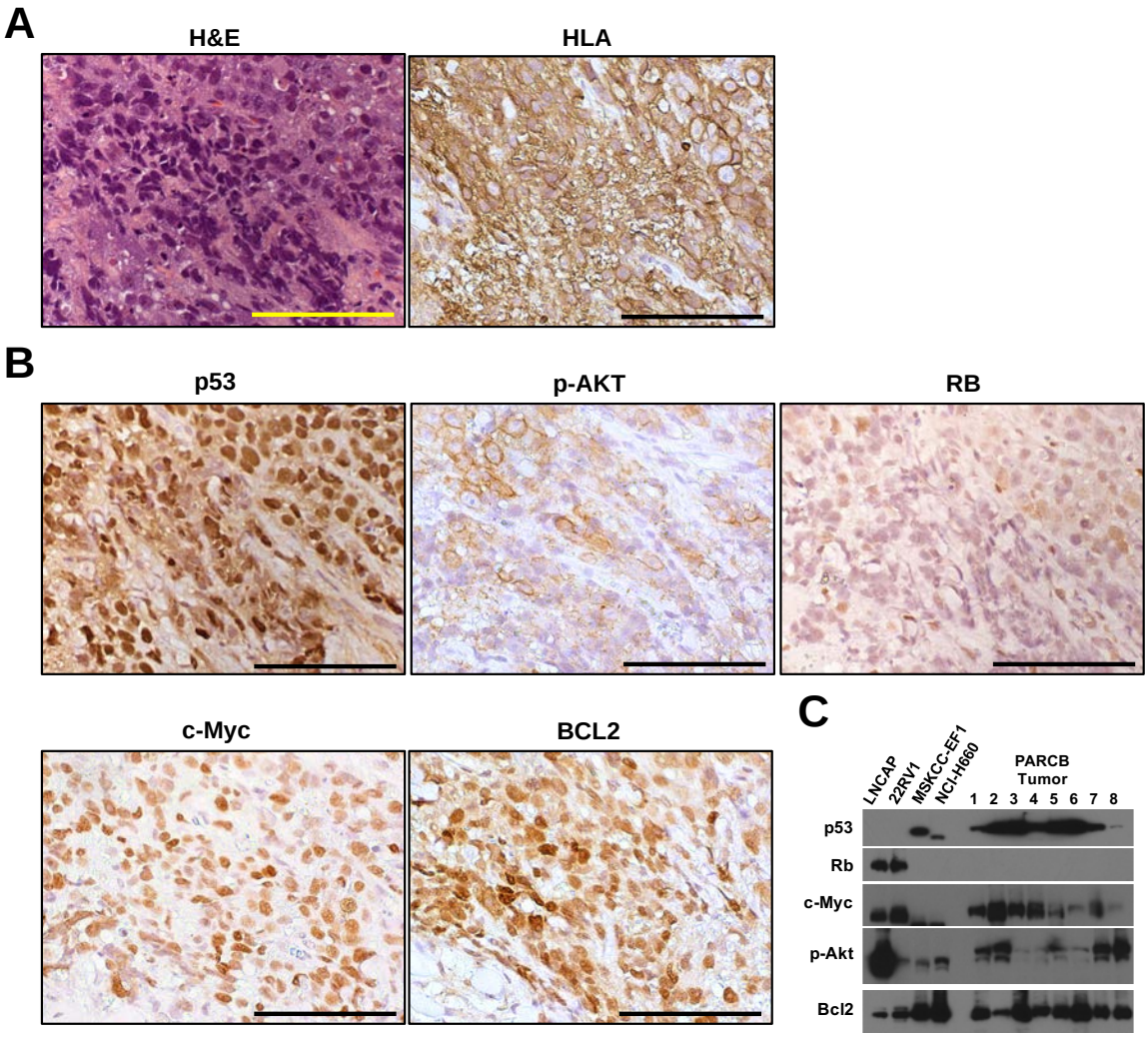

Fig. S1. PARCB tumors are of human origin and display expression of the five initiating genetic factors. (**A**) Representative H&E-stained image and IHC image for anti-HLA (Human Leukocyte Antigen) in PARCB tumors. (**B**) Photomicrographs of PARCB tumors with IHC staining for p53, phospho-AKT S473 (p-AKT), RB, c-Myc, and BCL2. Scale bar=100µm. (**C**) Immunoblots of patient-derived prostate cancer cell lines and PARCB tumors with antibodies against p53, RB, c-Myc, p-AKT, and BCL2. LNCAP and 22RV1 cell lines are representatives of PrAd. MSKCC-EF1 and NCI-H660 cell lines are representatives of SCPC.

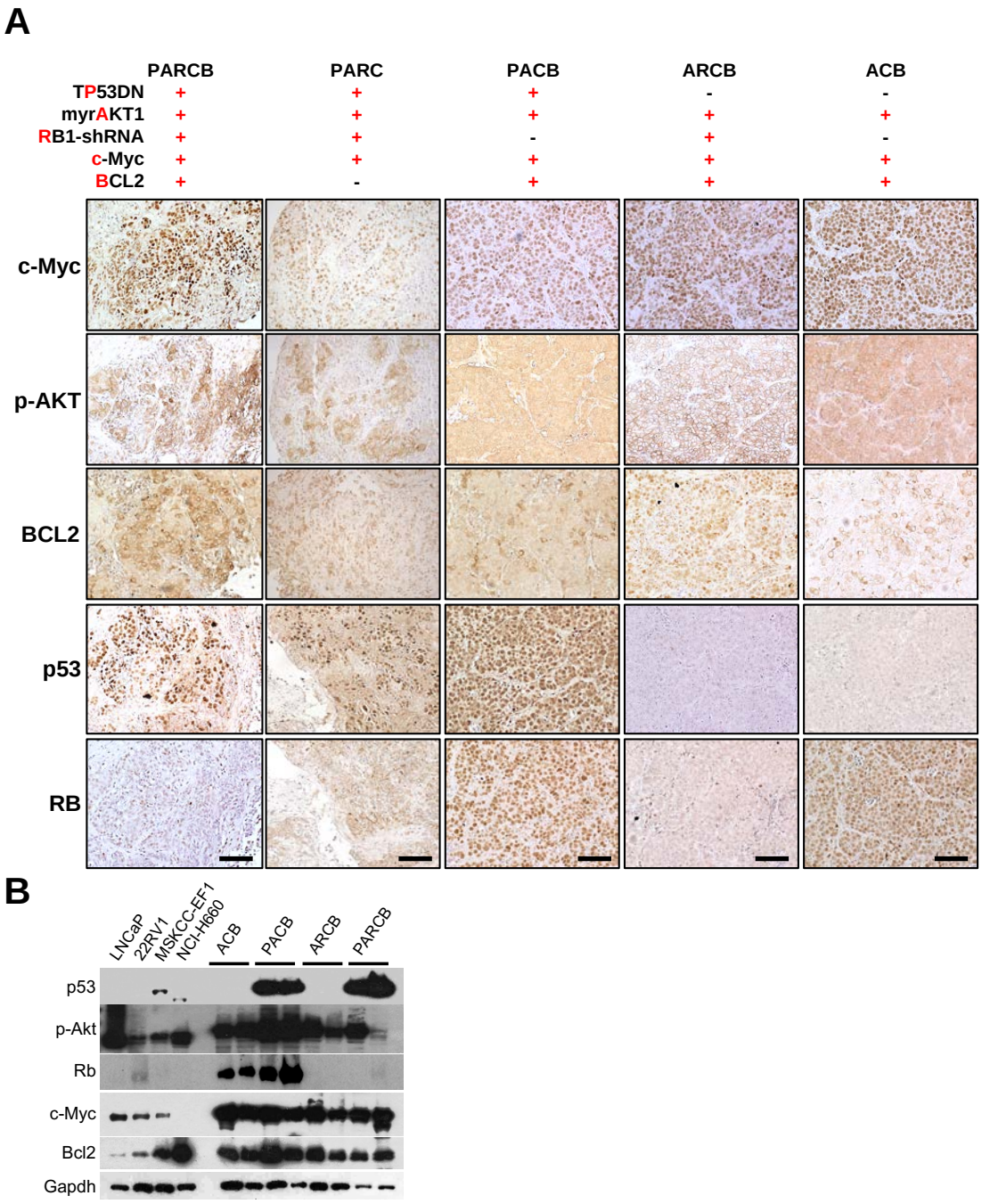

Fig. S2. Engineered tumor models display expression of genetic drivers. (**A**) Photomicrographs of xenograft grafts driven by different gene combinations with IHC staining for p53, RB, c-Myc, p-AKT, and BCL2. PARCB=5 gene combination, PACB with no *RB1*-shRNA, ARCB with no dominant negative p53, and ACB with no *RB1*-shRNA and no dominant negative p53. Scale bar=100µm. (**B**) Representative immunoblots of engineered tumor cell lines with antibodies against five genetic drivers; p53, p-AKT, RB, c-Myc, and BCL2. GAPDH (Glyceraldehyde-3-Phosphate Dehydrogenase) was used as a loading control. LNCAP and 22RV1 are PrAd cell lines. MSKCC-EF1 and NCI-H660 are SCPC cell lines.

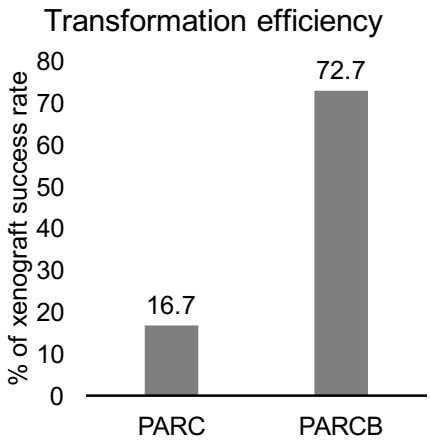

	Xenograft	No xenograft	Total
PARC	2	10	12
PARCB	8	3	11
Total	10	13	

Fig. S3. BCL2 overexpression enhances the efficiency of lentivirally-transduced organoid formation and *in vivo* tumor development. Graph (Left) and table (Right) showing the efficiency of xenograft development in immunodeficient NOD/SCID-IL2R-γc-KO mice with or without BCL2 overexpression. PARC is no BCL2 overexpression. BCLl2 overexpression in PARCB significantly increased the success rate of tumor outgrowth (P=0.01, two-sided Fisher's exact test).

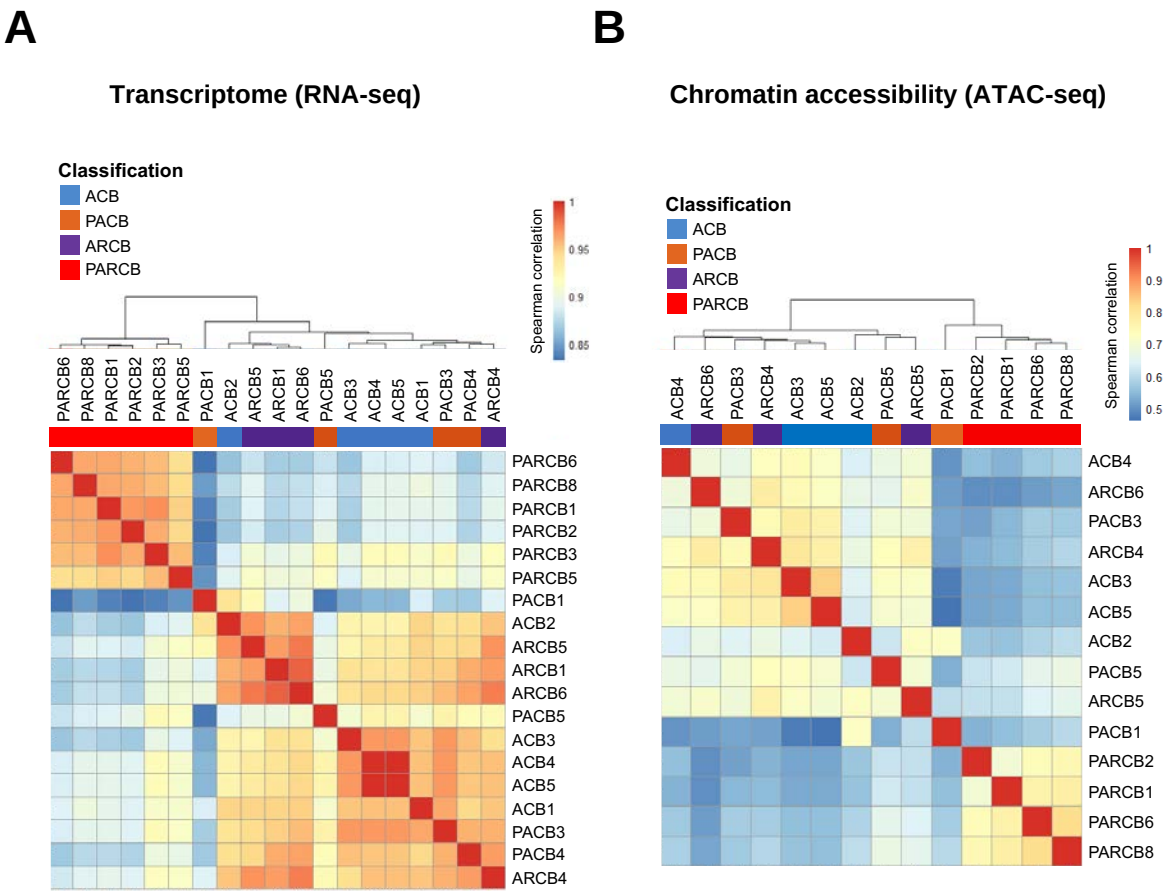

Fig. S4. PARCB cell lines have distinct transcriptional and chromatin-accessibility landscapes compared to ACB, PACB, and ARCB cell lines. Unsupervised hierarchical clustering demonstrated that PARCB cell lines clustered together and the other ACB, PACB, and ARCB cell lines showed mixed correlations in datasets of RNA-seq (**A**) and ATAC-seq (**B**). The color bar is indicating a distance (0=the closest and 1=the farthest).

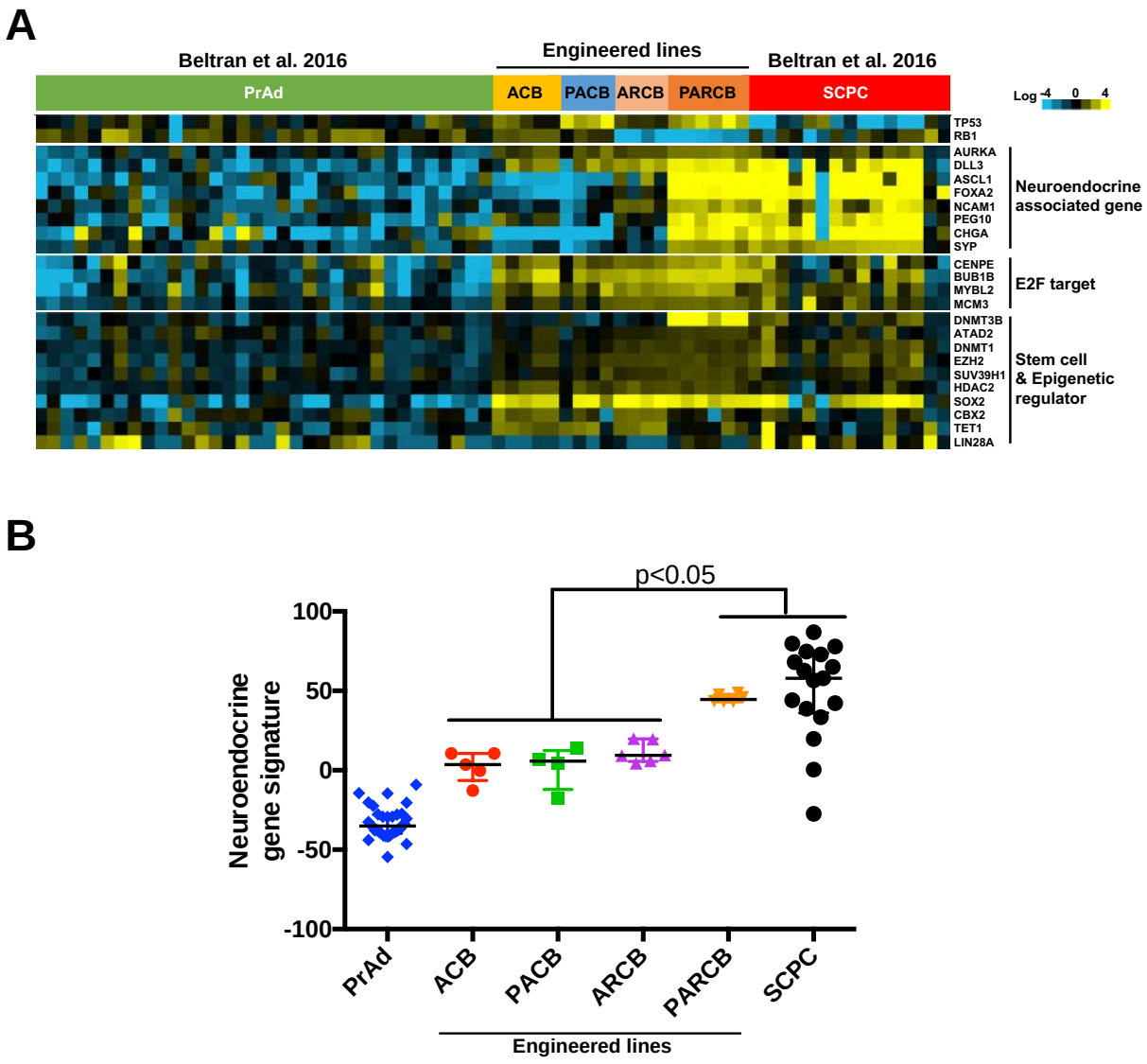

Fig. S5. PARCB lines are similar to human SCPC. (**A**) Expression of 22 SCPC-specific genes in RNA-seq data of the engineered tumor cell lines: PARCB, PACB, ARCB, and ACB lines. The gene set was selected in *Ku et al.*, 2017. The gene expression of prostate cancer patient samples (PrAd and SCPC) was obtained from *Beltran et al.*, 2016 RNA-seq dataset. (**B**) Neuroendocrine gene signature scores (developed by *Beltran et al.*, 2016) for engineered tumor lines (ACB, PACB, ARCB, and PARCB) and human patient samples (PrAd and SCPC). Median with interquartile range. Dots represent individual samples. Bars represent the median with interquartile range.

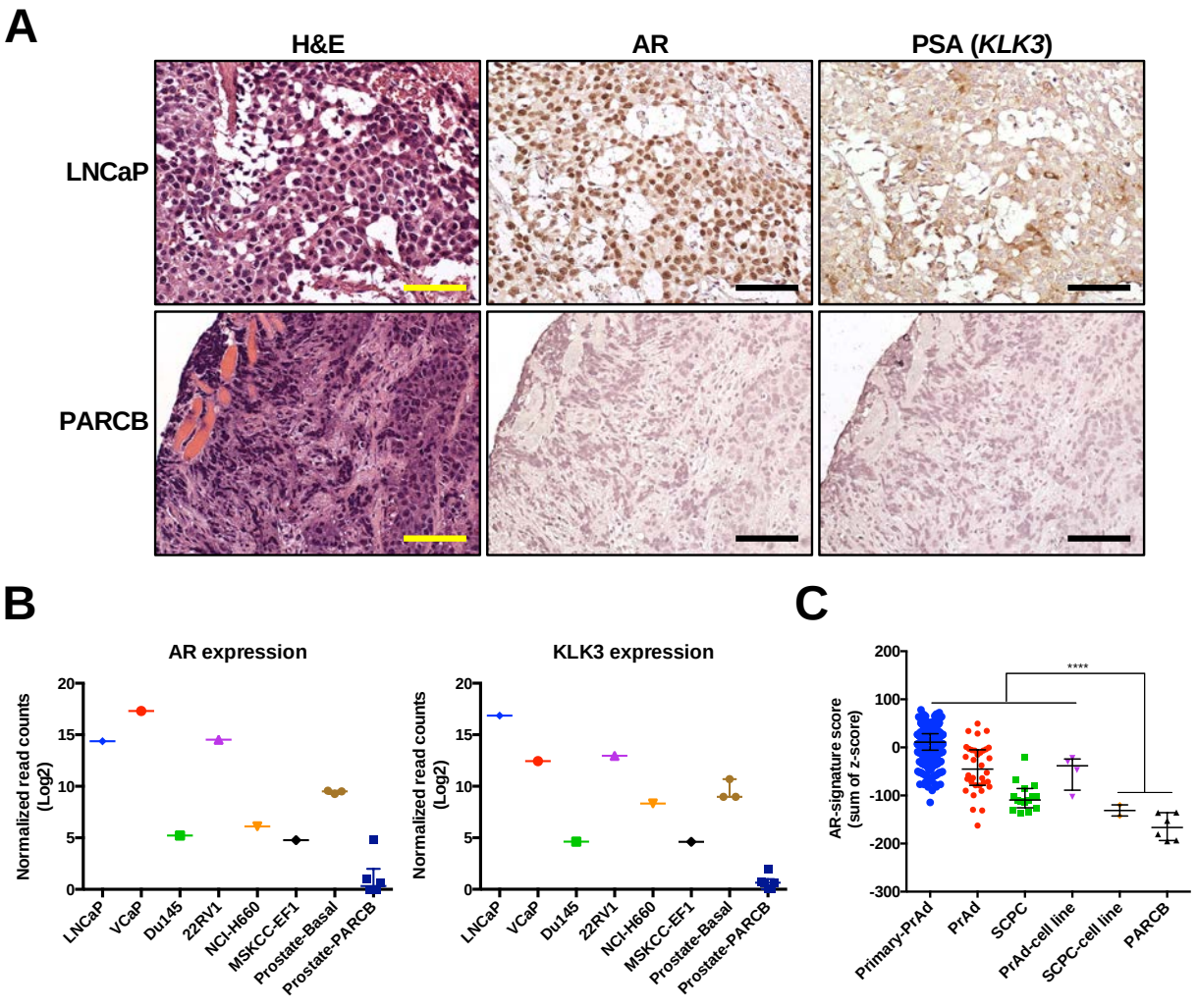

Fig. S6. Androgen receptor signaling in PARCB cell lines are androgen receptor independent and chemotherapy-sensitive. (**A**) Immunohistochemistry staining with antibodies against androgen receptor (AR) and prostate specific antigen (PSA, encoded by *KLK3* gene). LNCaP was used for positive controls for AR and PSA staining. Scale bar=100μm. (**B**) Gene expression level of *AR* and *KLK3* in prostate cancer cell lines, prostate basal epithelial cells, and prostate-PARCB cell lines. Y-axis is normalized read counts from RNA-seq data. Mean with standard error of the mean. (**C**) AR-associated gene signature scores of primary prostate adenocarcinoma (Primary-PrAd), castration-resistant prostate adenocarcinoma (PrAd), castration-resistant small cell prostate cancer (SCPC), patient-derived cell lines from adenocarcinoma and small cell prostate cancer (PrAd-cell line and SCPC-cell lines), and PARCB cell lines. Primary-PrAd samples were from TCGA datasets. PrAd and SCPC were from *Beltran et al., 2016* dataset. Median with interquartile range. ****=P<0.0001 (t-test). Details are described in materials and methods.

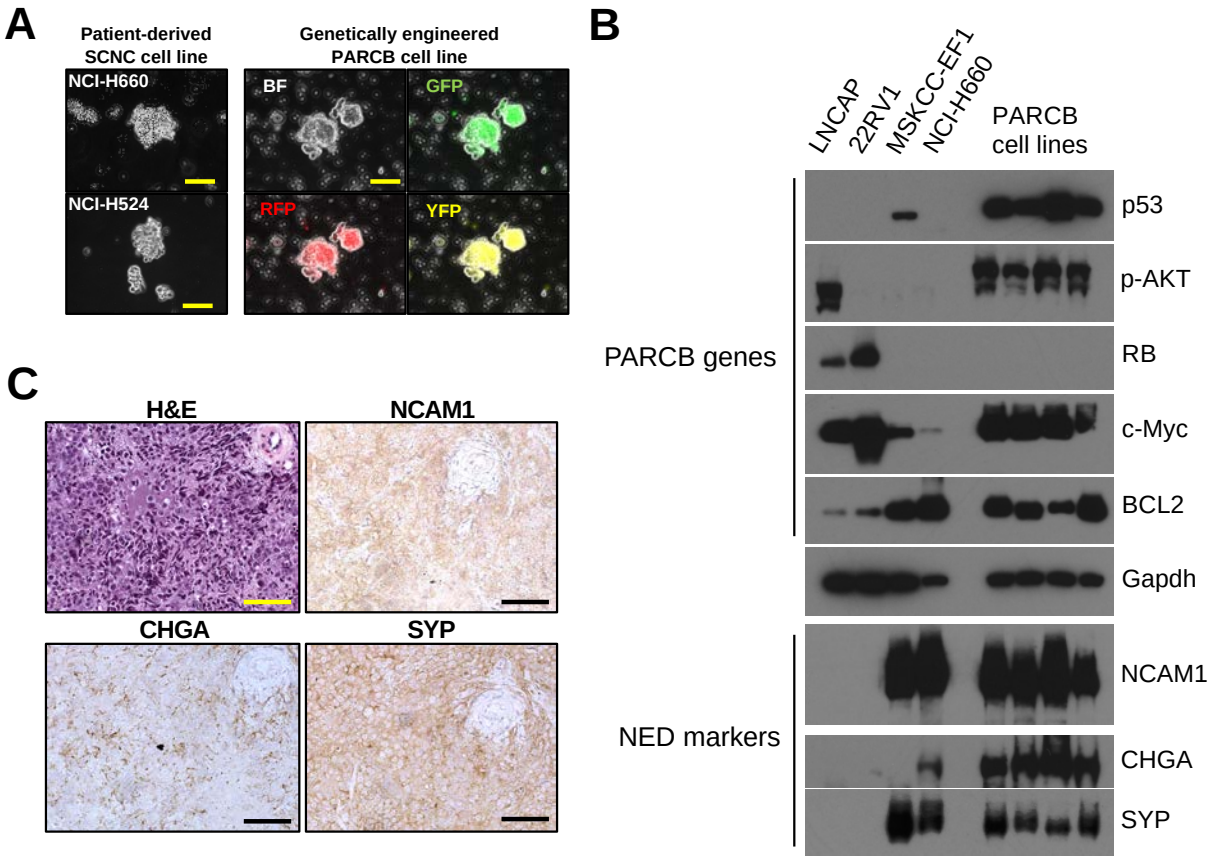

Fig. S7. PARCB tumor cell lines mirror human SCPC features. (**A**) Representative morphologic images of patient-derived SCPC (NCI-H660), SCLC (NCI-H524) and PARCB tumor cell lines *in vitro* 2D culture. BF=Bright field. Scale bar=200μm. (**B**) Immunoblots with antibodies against five genetic drivers; p53, p-AKT, RB, c-Myc, BCL2 and NED markers; NCAM1, CHGA, and SYP in multiple PARCB cell lines. GAPDH (Glyceraldehyde-3-Phosphate Dehydrogenase) was used as a loading control. LNCAP and 22RV1 are PrAd cell lines. MSKCC-EF1 and NCI-H660 are SCPC cell lines. (**C**) Photomicrographs of xenografts derived from PARCB cell lines with H&E staining and IHC staining for NED markers. Scale bar=100μm.

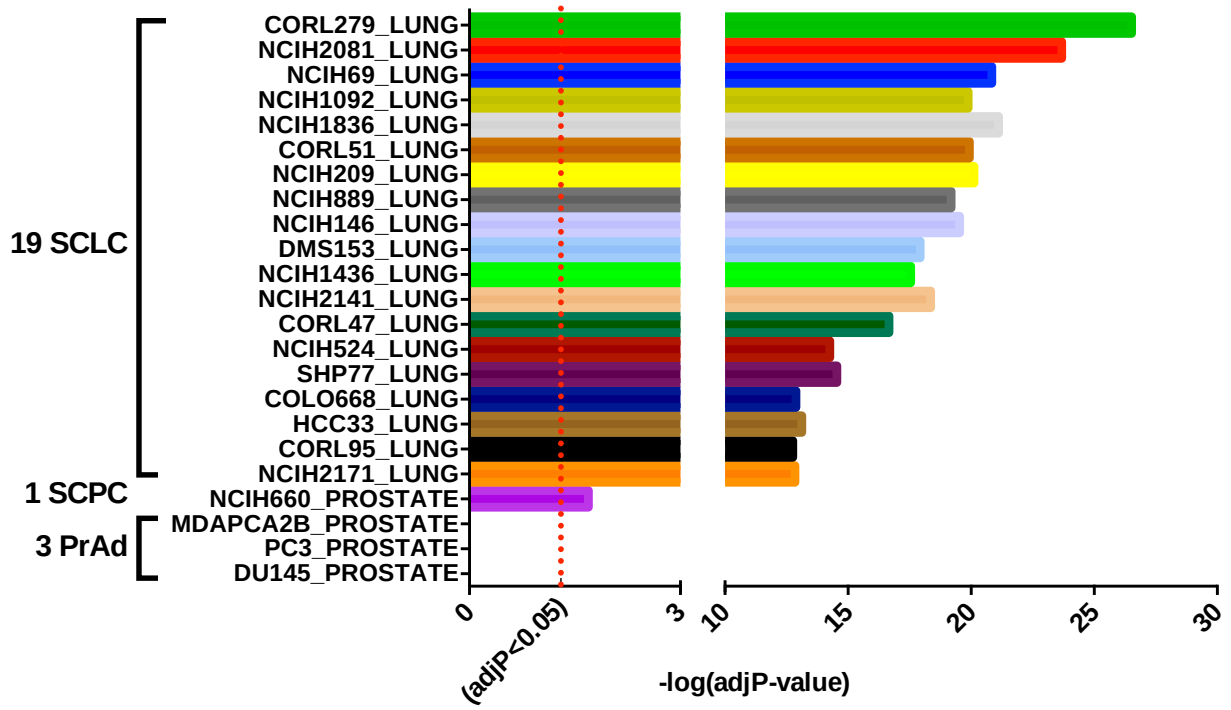

Fig. S8. PARCB cell lines have a strong transcriptional similarity to SCLC as well as SCPC cell lines. Computational analysis tool (DESeq2) identified 1232 up-regulated genes (>2 log fold change, adjusted P<0.01, described in materials and methods, and table S2) in PARCB cell lines compared to patient-derived PrAd lines (LNCaP, 22RV1, and VCaP). Using the gene list, gene list enrichment analysis (Enrichr, http://amp.pharm.mssm.edu/Enrichr) identified that the top 19 cancer cell lines which were all SCLC cell lines and 1 SCPC (NCI-H660) cell line were significantly shared genes in the list with PARCB cell lines (table S4).

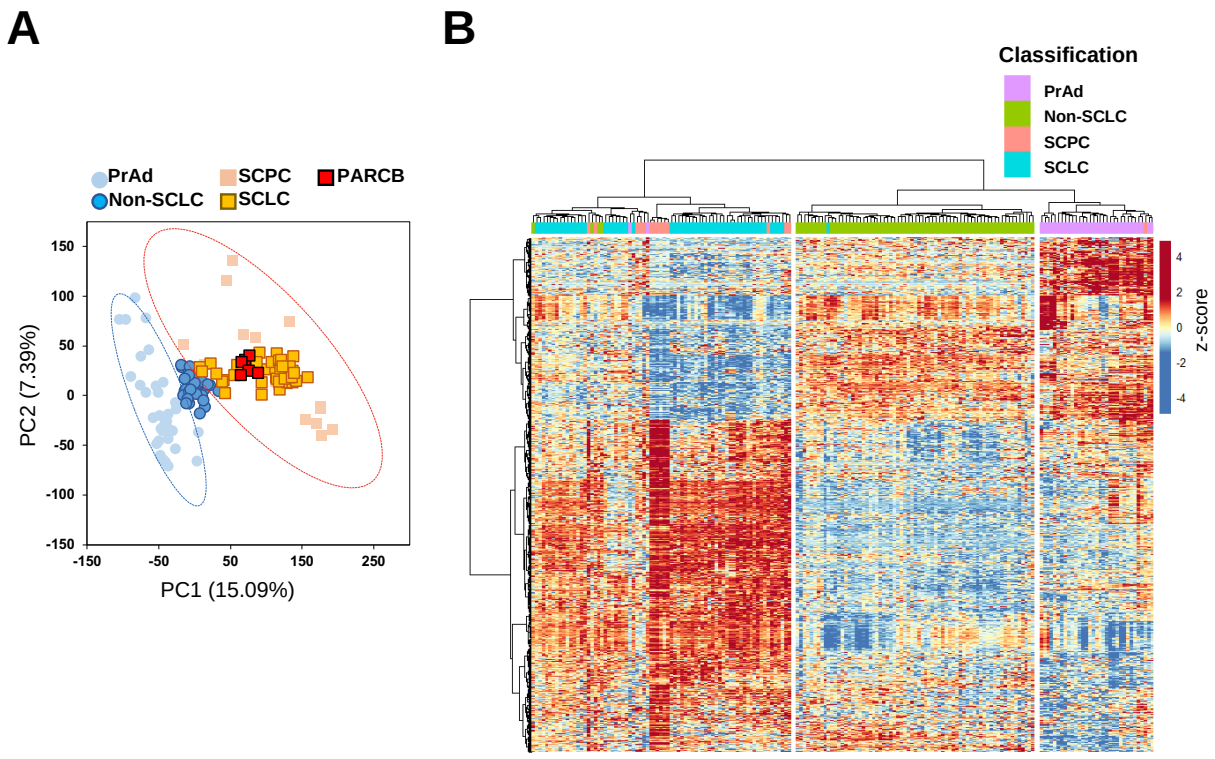

Fig. S9. SCPC and SCLC have a significantly similar transcriptional profile which is distinct from other cancer phenotypes. (**A**) SCLC and non-SCLC patient samples from were projected to prostate PLSR plot using gene expression data (RNA-seq). (**B**) 1726 genes were ranked by t-test P-value (P<0.001) on a prostate PrAd vs SCPC comparison in *Beltran et al., 2016*. These selected genes were used to perform the clustering analysis (Euclidean distance, described in materials and methods) across lung and prostate cancer datasets (*Beltran et al., 2016*, *George et al., 2015*, TCGA). The heat-map was generated with scaled z-score of the genes.

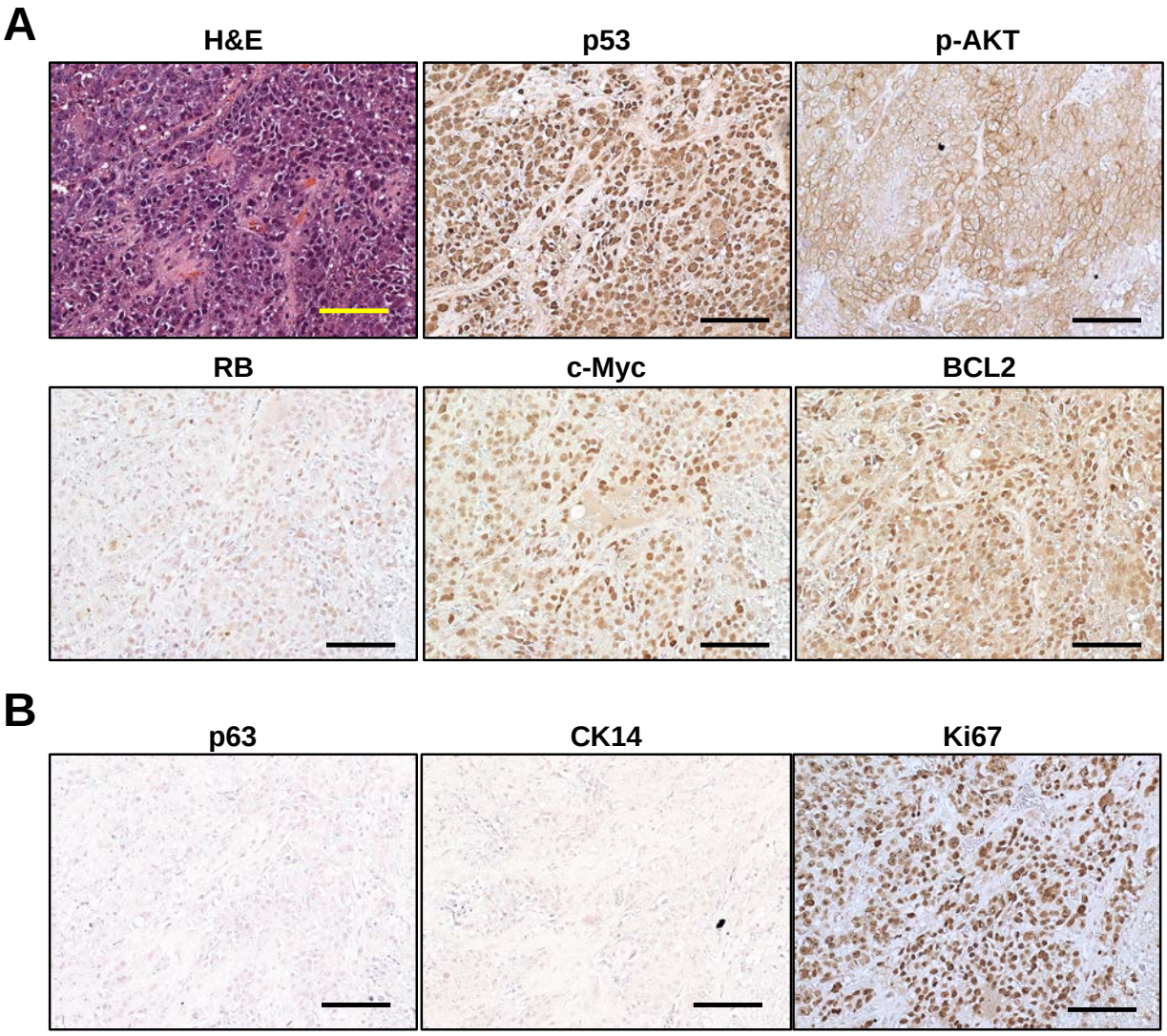

Fig. S10. NHBE-PARCB tumors express the five genetic drivers and epithelial differentiation and proliferation markers. (**A**) Photomicrographs of NHBE-PARCB tumors with H&E and IHC staining with antibodies against p53, p-AKT, RB, c-Myc, and BCL2. (**B**) Representative IHC images with anti-epithelial cell markers p63, cytokeratin 14 (CK14), and anti-proliferation marker Ki67. Scale bar=100μm.

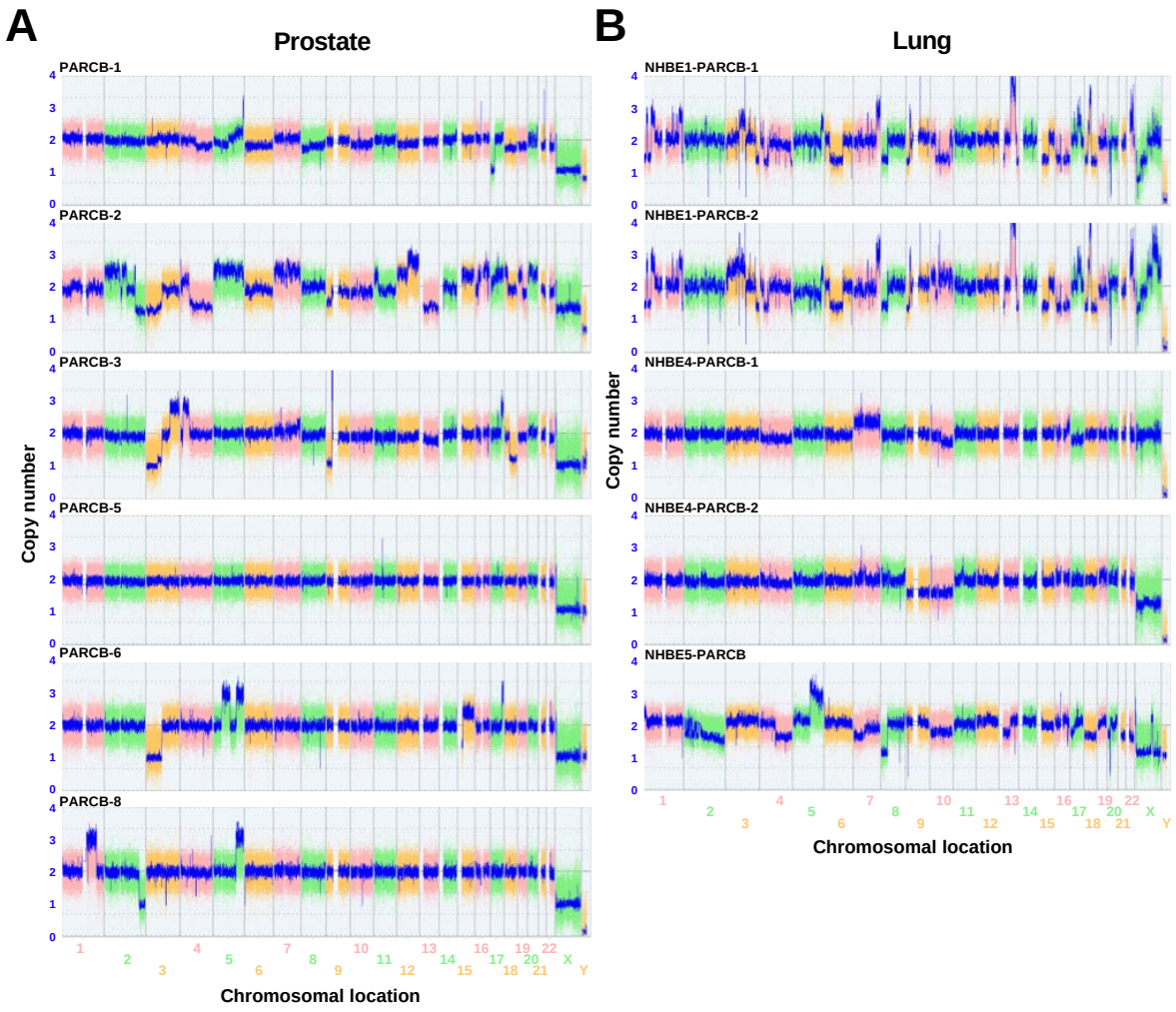

Fig. S11. Prostate- and Lung-PARCB cell lines have no common genomic alterations. Whole genome comparative genomic hybridization (CGH) array plots showing chromosomal locations and copy number alterations of PARCB cell lines of the prostate (**A**) and the lung (**B**) analyzed using the high-resolution Affymetrix CytoScanHD platform. The blue colored line represents the smoothed copy number profile.

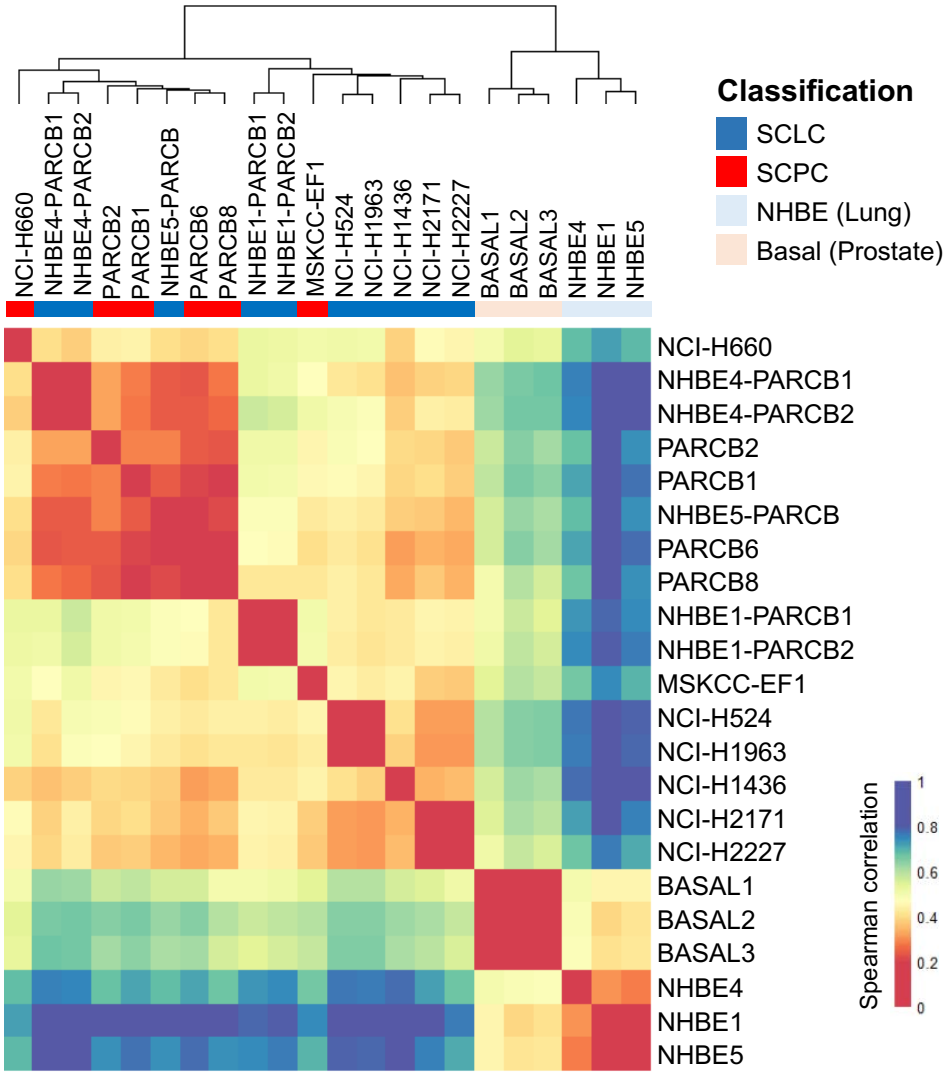

Fig. S12. SCPC and SCLC have similar chromatin-accessibility landscapes. Unsupervised hierarchical clustering showed two clusters; one includes lung and prostate PARCB cell lines and SCNC cell lines (two SCPC, NCI-H660 and EF1, and five SCLC, NCI-H1436, -H2171, -H2227, -H524, and -H1963, cell lines) and the other includes two distinct normal epithelial cells from lung (NHBE) and prostate (Basal). The color bar is indicating a distance (0=the closest and 1=the farthest).

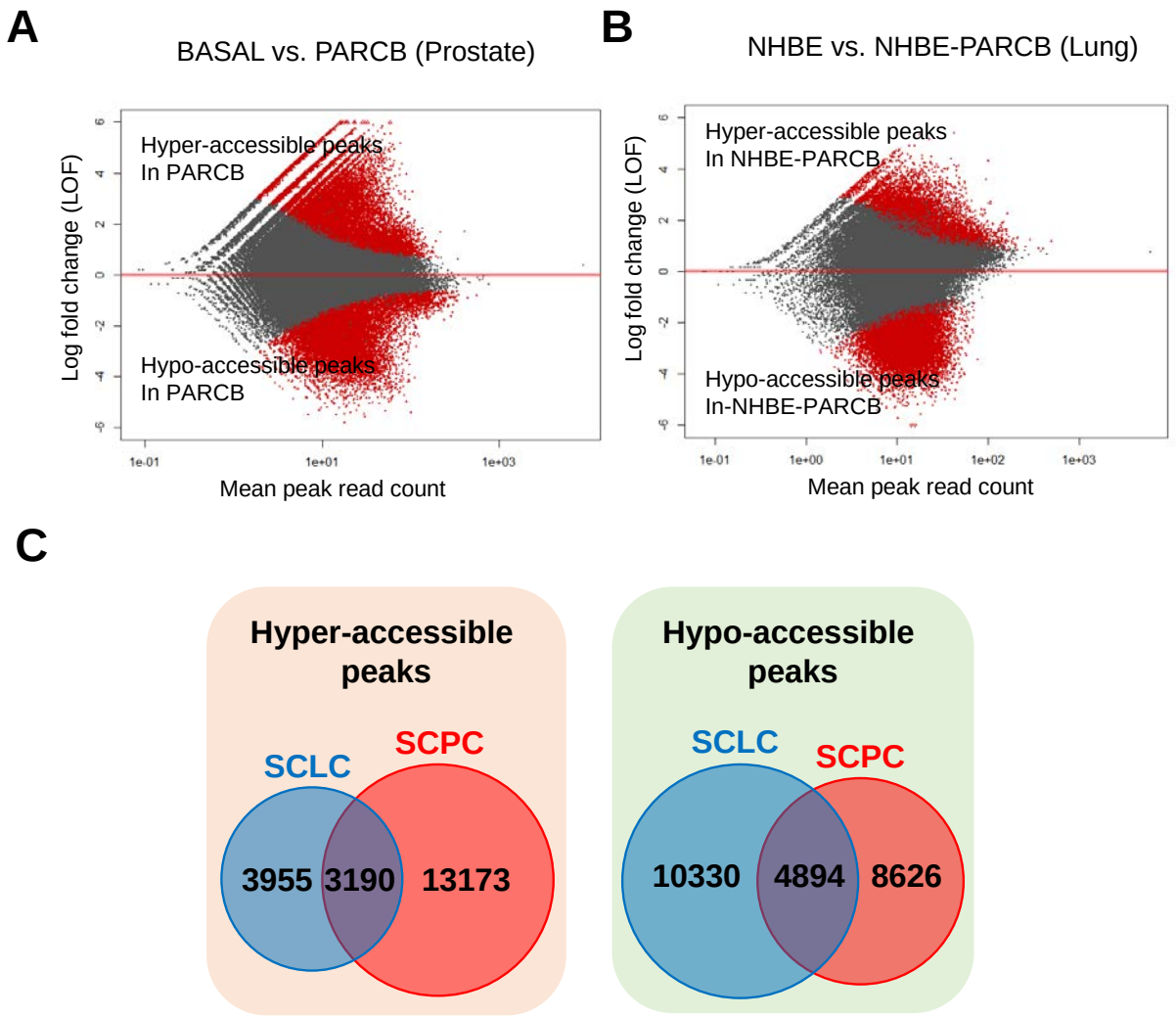

Fig. S13. SCPC and SCLC significantly share hyper- and hypo-accessible chromatin regions. Hyper- and hypo-accessible peaks were isolated by using DESeq2 (adjusted P<0.05) between PARCB transformants and normal epithelial cells in prostate (**A**) and lung (**B**). (**C**) Hyper- and hypo-accessible peaks in lung and prostate PARCB cell lines compared to normal lung and prostate epithelial cells. Venn diagram showing the numbers of shared hyper- and hypo-accessible peaks in prostate and lung PARCB tumors. The overlaps of differential accessible peaks in the lung and prostate were statistically significant (P<0.001).

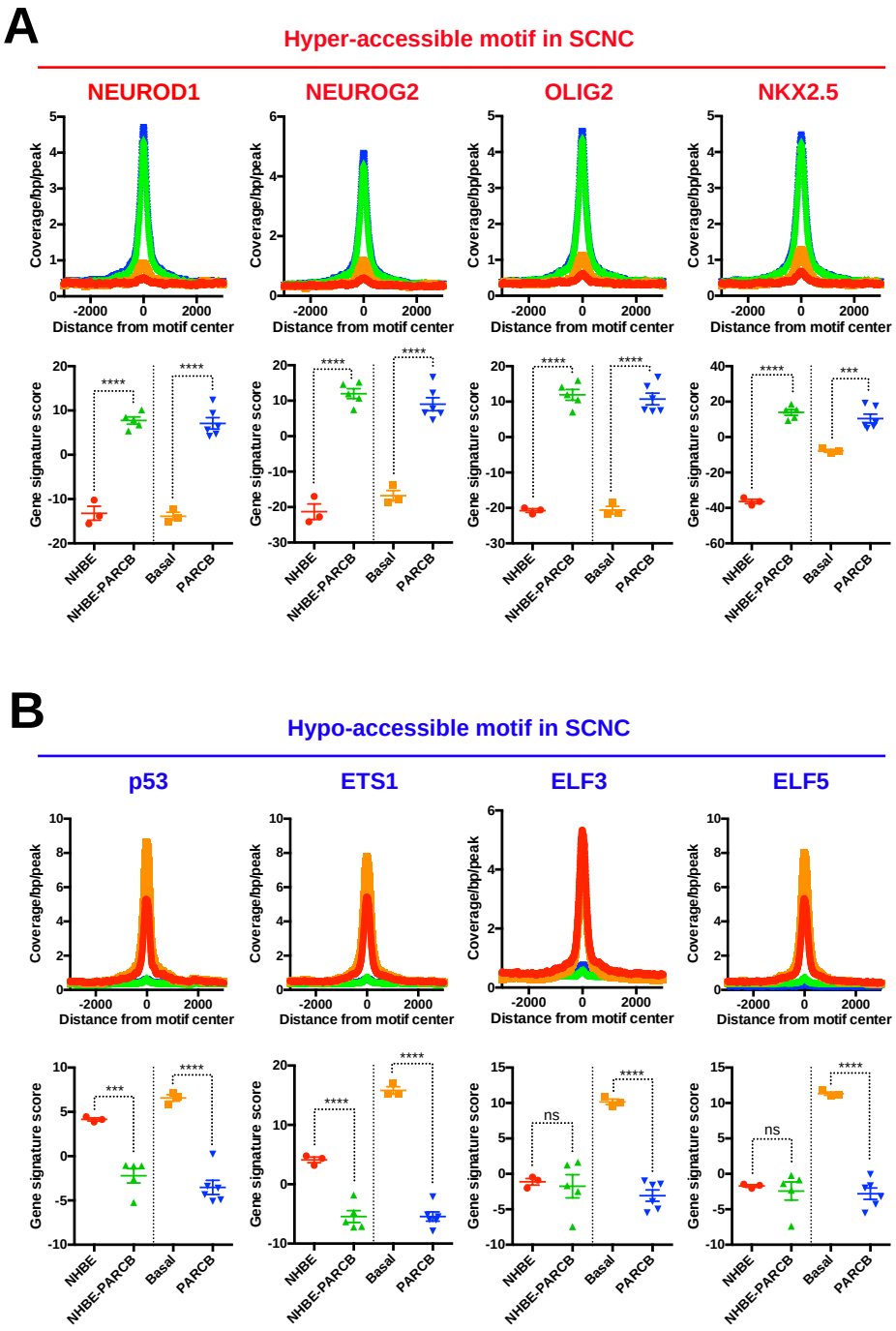

Fig. S14. Differentially accessible TF motifs correlated with the transcriptional output of TF target genes for each motif. (Top) Selected visualization of ATAC-seq footprint for (**A**) hyper- or (**B**) hypo-accessible TF motifs. (Bottom) The transcriptional activities of the TF motifs were measured by gene signature scores (Y-axis) which are generated by expression sum of z-score of signature genes associated with their motifs. The X-axis shows NHBE, NHBE-PARCB, primary prostate basal epithelial, and PARCB cells. Median with interquartile range. ***=P<0.001, ****=P<0.0001, ns=P>0.05 (one-way ANOVA). The computational analyses are described in materials and methods.

References and Notes

1. D. Hanahan, R. A. Weinberg, Hallmarks of cancer: The next generation. *Cell* **144**, 646–674 (2011). doi:10.1016/j.cell.2011.02.013 Medline

2. R. Nadal, M. Schweizer, O. N. Kryvenko, J. I. Epstein, M. A. Eisenberger, Small cell carcinoma of the prostate. *Nat. Rev. Urol.* **11**, 213–219 (2014). doi:10.1038/nrurol.2014.21 Medline

3. A. F. Gazdar, P. A. Bunn, J. D. Minna, Small-cell lung cancer: What we know, what we need to know and the path forward. *Nat. Rev. Cancer* **17**, 765 (2017). doi:10.1038/nrc.2017.106 Medline

4. L. V. Sequist, B. A. Waltman, D. Dias-Santagata, S. Digumarthy, A. B. Turke, P. Fidias, K. Bergethon, A. T. Shaw, S. Gettinger, A. K. Cosper, S. Akhavanfard, R. S. Heist, J. Temel, J. G. Christensen, J. C. Wain, T. J. Lynch, K. Vernovsky, E. J. Mark, M. Lanuti, A. J. Iafrate, M. Mino-Kenudson, J. A. Engelman, Genotypic and histological evolution of lung cancers acquiring resistance to EGFR inhibitors. *Sci. Transl. Med.* **3**, 75ra26 (2011). doi:10.1126/scitranslmed.3002003 Medline

5. H. L. Tan, A. Sood, H. A. Rahimi, W. Wang, N. Gupta, J. Hicks, S. Mosier, C. D. Gocke, J. I. Epstein, G. J. Netto, W. Liu, W. B. Isaacs, A. M. De Marzo, T. L. Lotan, Rb loss is characteristic of prostatic small cell neuroendocrine carcinoma. *Clin. Cancer Res.* **20**, 890–903 (2014). doi:10.1158/1078-0432.CCR-13-1982 Medline

6. M. J. Niederst, L. V. Sequist, J. T. Poirier, C. H. Mermel, E. L. Lockerman, A. R. Garcia, R. Katayama, C. Costa, K. N. Ross, T. Moran, E. Howe, L. E. Fulton, H. E. Mulvey, L. A. Bernardo, F. Mohamoud, N. Miyoshi, P. A. VanderLaan, D. B. Costa, P. A. Jänne, D. R. Borger, S. Ramaswamy, T. Shioda, A. J. Iafrate, G. Getz, C. M. Rudin, M. Mino-Kenudson, J. A. Engelman, RB loss in resistant EGFR mutant lung adenocarcinomas that transform to small-cell lung cancer. *Nat. Commun.* **6**, 6377 (2015). doi:10.1038/ncomms7377 Medline

7. H. Beltran, D. Prandi, J. M. Mosquera, M. Benelli, L. Puca, J. Cyrta, C. Marotz, E. Giannopoulou, B. V. S. K. Chakravarthi, S. Varambally, S. A. Tomlins, D. M. Nanus, S. T. Tagawa, E. M. Van Allen, O. Elemento, A. Sboner, L. A. Garraway, M. A. Rubin, F. Demichelis, Divergent clonal evolution of castration-resistant neuroendocrine prostate cancer. *Nat. Med.* **22**, 298–305 (2016). doi:10.1038/nm.4045 Medline

8. S. Y. Ku, S. Rosario, Y. Wang, P. Mu, M. Seshadri, Z. W. Goodrich, M. M. Goodrich, D. P. Labbé, E. C. Gomez, J. Wang, H. W. Long, B. Xu, M. Brown, M. Loda, C. L. Sawyers, L. Ellis, D. W. Goodrich, Rb1 and Trp53 cooperate to suppress prostate cancer lineage plasticity, metastasis, and antiandrogen resistance. *Science* **355**, 78–83 (2017). doi:10.1126/science.aah4199 Medline

9. R. Fisher, S. Horswell, A. Rowan, M. P. Salm, E. C. de Bruin, S. Gulati, N. McGranahan, M. Stares, M. Gerlinger, I. Varela, A. Crockford, F. Favero, V. Quidville, F. André, C. Navas, E. Grönroos, D. Nicol, S. Hazell, D. Hrouda, T. O'Brien, N. Matthews, B. Phillimore, S. Begum, A. Rabinowitz, J. Biggs, P. A. Bates, N. Q. McDonald, G. Stamp, B. Spencer-Dene, J. J. Hsieh, J. Xu, L. Pickering, M. Gore, J. Larkin, C. Swanton, Development of synchronous VHL syndrome tumors reveals contingencies and constraints to tumor evolution. *Genome Biol.* **15**, 433 (2014). doi:10.1186/s13059-014-0433-z Medline

10. H. Chen, X. He, The convergent cancer evolution toward a single cellular destination. *Mol. Biol. Evol.* **33**, 4–12 (2016). doi:10.1093/molbev/msv212 Medline

11. N. McGranahan, C. Swanton, Clonal heterogeneity and tumor evolution: Past, present, and the future. *Cell* **168**, 613–628 (2017). doi:10.1016/j.cell.2017.01.018 Medline

12. T. Stoyanova, A. R. Cooper, J. M. Drake, X. Liu, A. J. Armstrong, K. J. Pienta, H. Zhang, D. B. Kohn, J. Huang, O. N. Witte, A. S. Goldstein, Prostate cancer originating in basal cells progresses to adenocarcinoma propagated by luminal-like cells. *Proc. Natl. Acad. Sci. U.S.A.* **110**, 20111–20116 (2013). doi:10.1073/pnas.1320565110 Medline

13. V. Parimi, R. Goyal, K. Poropatich, X. J. Yang, Neuroendocrine differentiation of prostate cancer: A review. *Am. J. Clin. Exp. Urol.* **2**, 273–285 (2014). Medline

14. J. K. Lee, J. W. Phillips, B. A. Smith, J. W. Park, T. Stoyanova, E. F. McCaffrey, R. Baertsch, A. Sokolov, J. G. Meyerowitz, C. Mathis, D. Cheng, J. M. Stuart, K. M. Shokat, W. C. Gustafson, J. Huang, O. N. Witte, N-Myc drives neuroendocrine prostate cancer initiated from human prostate epithelial cells. *Cancer Cell* **29**, 536–547 (2016). doi:10.1016/j.ccell.2016.03.001 Medline

15. Y. Lin, J. Fukuchi, R. A. Hiipakka, J. M. Kokontis, J. Xiang, Up-regulation of Bcl-2 is required for the progression of prostate cancer cells from an androgen-dependent to an androgen-independent growth stage. *Cell Res.* **17**, 531–536 (2007). doi:10.1038/cr.2007.12 Medline

16. M. Krajewska, S. Krajewski, J. I. Epstein, A. Shabaik, J. Sauvageot, K. Song, S. Kitada, J. C. Reed, Immunohistochemical analysis of bcl-2, bax, bcl-X, and mcl-1 expression in prostate cancers. *Am. J. Pathol.* **148**, 1567–1576 (1996). Medline

17. L. D. Shultz, F. Ishikawa, D. L. Greiner, Humanized mice in translational biomedical research. *Nat. Rev. Immunol.* **7**, 118–130 (2007). doi:10.1038/nri2017 Medline

18. P. Mu, Z. Zhang, M. Benelli, W. R. Karthaus, E. Hoover, C.-C. Chen, J. Wongvipat, S.-Y. Ku, D. Gao, Z. Cao, N. Shah, E. J. Adams, W. Abida, P. A. Watson, D. Prandi, C.-H. Huang, E. de Stanchina, S. W. Lowe, L. Ellis, H. Beltran, M. A. Rubin, D. W. Goodrich, F. Demichelis, C. L. Sawyers, SOX2 promotes lineage plasticity and antiandrogen resistance in TP53- and RB1-deficient prostate cancer. *Science* **355**, 84–88 (2017). doi:10.1126/science.aah4307 Medline

19. M. Zou, R. Toivanen, A. Mitrofanova, N. Floch, S. Hayati, Y. Sun, C. Le Magnen, D. Chester, E. A. Mostaghel, A. Califano, M. A. Rubin, M. M. Shen, C. Abate-Shen, Transdifferentiation as a mechanism of treatment resistance in a mouse model of castration-resistant prostate cancer. *Cancer Discov.* **7**, 736–749 (2017). doi:10.1158/2159-8290.CD-16-1174 Medline

20. E. Y. Chen, C. M. Tan, Y. Kou, Q. Duan, Z. Wang, G. V. Meirelles, N. R. Clark, A. Ma'ayan, Enrichr: Interactive and collaborative HTML5 gene list enrichment analysis tool. *BMC Bioinformatics* **14**, 128 (2013). doi:10.1186/1471-2105-14-128 Medline

21. J. George, J. S. Lim, S. J. Jang, Y. Cun, L. Ozretić, G. Kong, F. Leenders, X. Lu, L. Fernández-Cuesta, G. Bosco, C. Müller, I. Dahmen, N. S. Jahchan, K.-S. Park, D. Yang, A. N. Karnezis, D. Vaka, A. Torres, M. S. Wang, J. O. Korbel, R. Menon, S.-M. Chun, D. Kim, M. Wilkerson, N. Hayes, D. Engelmann, B. Pützer, M. Bos, S. Michels, I. Vlasic, D. Seidel, B. Pinther, P. Schaub, C. Becker, J. Altmüller, J. Yokota, T. Kohno, R. Iwakawa, K. Tsuta, M. Noguchi, T. Muley, H. Hoffmann, P. A. Schnabel, I. Petersen, Y. Chen, A. Soltermann, V. Tischler, C. M. Choi, Y.-H. Kim, P. P. Massion, Y. Zou, D. Jovanovic, M. Kontic, G. M. Wright, P. A. Russell, B. Solomon, I. Koch, M. Lindner, L. A. Muscarella, A. la Torre, J. K. Field, M. Jakopovic, J. Knezevic, E. Castaños-Vélez, L. Roz, U. Pastorino, O.-T. Brustugun, M. Lund-Iversen, E. Thunnissen, J. Köhler, M. Schuler, J. Botling, M. Sandelin, M. Sanchez-Cespedes, H. B. Salvesen, V. Achter,

U. Lang, M. Bogus, P. M. Schneider, T. Zander, S. Ansén, M. Hallek, J. Wolf, M. Vingron, Y. Yatabe, W. D. Travis, P. Nürnberg, C. Reinhardt, S. Perner, L. Heukamp, R. Büttner, S. A. Haas, E. Brambilla, M. Peifer, J. Sage, R. K. Thomas, Comprehensive genomic profiles of small cell lung cancer. *Nature* **524**, 47–53 (2015). doi:10.1038/nature14664 Medline

22. National Cancer Institute, The Cancer Genome Atlas; https://cancergenome.nih.gov/.

23. H. Zhang, J. Liu, P. T. Cagle, T. C. Allen, A. C. Laga, D. S. Zander, Distinction of pulmonary small cell carcinoma from poorly differentiated squamous cell carcinoma: An immunohistochemical approach. *Mod. Pathol.* **18**, 111–118 (2005). doi:10.1038/modpathol.3800251 Medline

24. J. Barretina, G. Caponigro, N. Stransky, K. Venkatesan, A. A. Margolin, S. Kim, C. J. Wilson, J. Lehár, G. V. Kryukov, D. Sonkin, A. Reddy, M. Liu, L. Murray, M. F. Berger, J. E. Monahan, P. Morais, J. Meltzer, A. Korejwa, J. Jané-Valbuena, F. A. Mapa, J. Thibault, E. Bric-Furlong, P. Raman, A. Shipway, I. H. Engels, J. Cheng, G. K. Yu, J. Yu, P. Aspesi Jr., M. de Silva, K. Jagtap, M. D. Jones, L. Wang, C. Hatton, E. Palescandolo, S. Gupta, S. Mahan, C. Sougnez, R. C. Onofrio, T. Liefeld, L. MacConaill, W. Winckler, M. Reich, N. Li, J. P. Mesirov, S. B. Gabriel, G. Getz, K. Ardlie, V. Chan, V. E. Myer, B. L. Weber, J. Porter, M. Warmuth, P. Finan, J. L. Harris, M. Meyerson, T. R. Golub, M. P. Morrissey, W. R. Sellers, R. Schlegel, L. A. Garraway, The Cancer Cell Line Encyclopedia enables predictive modelling of anticancer drug sensitivity. *Nature* **483**, 603–607 (2012). doi:10.1038/nature11003 Medline

25. W. K. Cheung, D. X. Nguyen, Lineage factors and differentiation states in lung cancer progression. *Oncogene* **34**, 5771–5780 (2015). doi:10.1038/onc.2015.85 Medline

26. W. A. Whyte, D. A. Orlando, D. Hnisz, B. J. Abraham, C. Y. Lin, M. H. Kagey, P. B. Rahl, T. I. Lee, R. A. Young, Master transcription factors and mediator establish super-enhancers at key cell identity genes. *Cell* **153**, 307–319 (2013). doi:10.1016/j.cell.2013.03.035 Medline

27. H. Osada, Y. Tatematsu, Y. Yatabe, Y. Horio, T. Takahashi, ASH1 gene is a specific therapeutic target for lung cancers with neuroendocrine features. *Cancer Res.* **65**, 10680–10685 (2005). doi:10.1158/0008-5472.CAN-05-1404 Medline

28. T. Jiang, B. J. Collins, N. Jin, D. N. Watkins, M. V. Brock, W. Matsui, B. D. Nelkin, D. W. Ball, Achaete-scute complex homologue 1 regulates tumor-initiating capacity in human small cell lung cancer. *Cancer Res.* **69**, 845–854 (2009). doi:10.1158/0008-5472.CAN-08-2762 Medline

29. J. K. Osborne, J. E. Larsen, M. D. Shields, J. X. Gonzales, D. S. Shames, M. Sato, A. Kulkarni, I. I. Wistuba, L. Girard, J. D. Minna, M. H. Cobb, NeuroD1 regulates survival and migration of neuroendocrine lung carcinomas via signaling molecules TrkB and NCAM. *Proc. Natl. Acad. Sci. U.S.A.* **110**, 6524–6529 (2013). doi:10.1073/pnas.1303932110 Medline

30. F. Guillemot, Spatial and temporal specification of neural fates by transcription factor codes. *Development* **134**, 3771–3780 (2007). doi:10.1242/dev.006379 Medline

31. S. N. Agoff, L. W. Lamps, A. T. Philip, M. B. Amin, R. A. Schmidt, L. D. True, A. L. Folpe, Thyroid transcription factor-1 is expressed in extrapulmonary small cell carcinomas but not in other extrapulmonary neuroendocrine tumors. *Mod. Pathol.* **13**, 238–242 (2000). doi:10.1038/modpathol.3880044 Medline

32. P. Remy, M. Baltzinger, The Ets-transcription factor family in embryonic development: Lessons from the amphibian and bird. *Oncogene* **19**, 6417–6431 (2000). doi:10.1038/sj.onc.1204044 Medline

33. B. Joseph, O. Hermanson, Molecular control of brain size: Regulators of neural stem cell life, death and beyond. *Exp. Cell Res.* **316**, 1415–1421 (2010). doi:10.1016/j.yexcr.2010.03.012 Medline

34. S. Heinz, C. Benner, N. Spann, E. Bertolino, Y. C. Lin, P. Laslo, J. X. Cheng, C. Murre, H. Singh, C. K. Glass, Simple combinations of lineage-determining transcription factors prime *cis*-regulatory elements required for macrophage and B cell identities. *Mol. Cell* **38**, 576–589 (2010). doi:10.1016/j.molcel.2010.05.004 Medline

35. L. Xin, D. A. Lawson, O. N. Witte, The Sca-1 cell surface marker enriches for a prostate-regenerating cell subpopulation that can initiate prostate tumorigenesis. *Proc. Natl. Acad. Sci. U.S.A.* **102**, 6942–6947 (2005). doi:10.1073/pnas.0502320102 Medline

36. S. Goel, M. J. DeCristo, A. C. Watt, H. BrinJones, J. Sceneay, B. B. Li, N. Khan, J. M. Ubellacker, S. Xie, O. Metzger-Filho, J. Hoog, M. J. Ellis, C. X. Ma, S. Ramm, I. E. Krop, E. P. Winer, T. M. Roberts, H.-J. Kim, S. S. McAllister, J. J. Zhao, CDK4/6 inhibition triggers anti-tumour immunity. *Nature* **548**, 471–475 (2017). doi:10.1038/nature23465 Medline

37. G. Tiscornia, O. Singer, I. M. Verma, Production and purification of lentiviral vectors. *Nat. Protoc.* **1**, 241–245 (2006). doi:10.1038/nprot.2006.37 Medline

38. A. S. Goldstein, J. M. Drake, D. L. Burnes, D. S. Finley, H. Zhang, R. E. Reiter, J. Huang, O. N. Witte, Purification and direct transformation of epithelial progenitor cells from primary human prostate. *Nat. Protoc.* **6**, 656–667 (2011). doi:10.1038/nprot.2011.317 Medline

39. J. Drost, W. R. Karthaus, D. Gao, E. Driehuis, C. L. Sawyers, Y. Chen, H. Clevers, Organoid culture systems for prostate epithelial and cancer tissue. *Nat. Protoc.* **11**, 347–358 (2016). doi:10.1038/nprot.2016.006 Medline

40. D. Gao, I. Vela, A. Sboner, P. J. Iaquinta, W. R. Karthaus, A. Gopalan, C. Dowling, J. N. Wanjala, E. A. Undvall, V. K. Arora, J. Wongvipat, M. Kossai, S. Ramazanoglu, L. P. Barboza, W. Di, Z. Cao, Q. F. Zhang, I. Sirota, L. Ran, T. Y. MacDonald, H. Beltran, J.-M. Mosquera, K. A. Touijer, P. T. Scardino, V. P. Laudone, K. R. Curtis, D. E. Rathkopf, M. J. Morris, D. C. Danila, S. F. Slovin, S. B. Solomon, J. A. Eastham, P. Chi, B. Carver, M. A. Rubin, H. I. Scher, H. Clevers, C. L. Sawyers, Y. Chen, Organoid cultures derived from patients with advanced prostate cancer. *Cell* **159**, 176–187 (2014). doi:10.1016/j.cell.2014.08.016 Medline

41. J. F. Lechner, M. A. LaVeck, A serum-free method for culturing normal human bronchial epithelial cells at clonal density. *J. Tissue Cult. Methods* **9**, 43–48 (1985). doi:10.1007/BF01797773

42. K. D. Mertz, S. R. Setlur, S. M. Dhanasekaran, F. Demichelis, S. Perner, S. Tomlins, J. Tchinda, B. Laxman, R. L. Vessella, R. Beroukhim, C. Lee, A. M. Chinnaiyan, M. A. Rubin, Molecular characterization of TMPRSS2-ERG gene fusion in the NCI-H660 prostate cancer cell line: A new perspective for an old model. *Neoplasia* **9**, 200–206 (2007). doi:10.1593/neo.07103 Medline

43. A. F. Gazdar, D. N. Carney, E. K. Russell, H. L. Sims, S. B. Baylin, P. A. Bunn Jr., J. G. Guccion, J. D. Minna, Establishment of continuous, clonable cultures of small-cell carcinoma of lung which have amine precursor uptake and decarboxylation cell properties. *Cancer Res.* **40**, 3502–3507 (1980). Medline

44. B.-H. Mevik, R. Wehrens, The pls package: Principal component and partial least squares regression in R. *J. Stat. Softw.* **18**, 23 (2007). doi:10.18637/jss.v018.i02

45. J. D. Buenrostro, P. G. Giresi, L. C. Zaba, H. Y. Chang, W. J. Greenleaf, Transposition of native chromatin for fast and sensitive epigenomic profiling of open chromatin, DNA-binding proteins and nucleosome position. *Nat. Methods* **10**, 1213–1218 (2013). doi:10.1038/nmeth.2688 Medline

46. A. R. Quinlan, I. M. Hall, BEDTools: A flexible suite of utilities for comparing genomic features. *Bioinformatics* **26**, 841–842 (2010). doi:10.1093/bioinformatics/btq033 Medline

47. M. I. Love, W. Huber, S. Anders, Moderated estimation of fold change and dispersion for RNA-seq data with DESeq2. *Genome Biol.* **15**, 550 (2014). doi:10.1186/s13059-014-0550-8 Medline

48. G. Wang, S. J. Jones, M. A. Marra, M. D. Sadar, Identification of genes targeted by the androgen and PKA signaling pathways in prostate cancer cells. *Oncogene* **25**, 7311–7323 (2006). doi:10.1038/sj.onc.1209715 Medline

49. P. S. Nelson, N. Clegg, H. Arnold, C. Ferguson, M. Bonham, J. White, L. Hood, B. Lin, The program of androgen-responsive genes in neoplastic prostate epithelium. *Proc. Natl. Acad. Sci. U.S.A.* **99**, 11890–11895 (2002). doi:10.1073/pnas.182376299 Medline

50. K. Wang, M. Li, H. Hakonarson, ANNOVAR: Functional annotation of genetic variants from high-throughput sequencing data. *Nucleic Acids Res.* **38**, e164 (2010). doi:10.1093/nar/gkq603 Medline